Commun. Comput. Phys.
doi: 10.4208/cicp.OA-2024-0159

Vol. **39**, No. 5, pp. 1363-1404
May 2026

The Implicit Unified Gas Kinetic Scheme for Neutron Transport with Arbitrary Anisotropic Scattering Model

Shuang Tan[1], Wenjun Sun[1] and Junxia Wei[1,*]

[1] *Institute of Applied Physics and Computational Mathematics, Haidian District, Beijing 100094, P.R. China.*

Received 14 July 2024; Accepted (in revised version) 23 March 2025

Abstract. In previous work, we developed the unified gas dynamics scheme (UGKS) and its corresponding time-implicit variant (IUGKS) for neutron transport. The multi-scale characteristics of these schemes are particularly well-suited for transport equations, which show good performances in large-scale conditions. However, only the isotropic scattering model equation was considered in these studies, which does not meet the application requirements in complex engineering cases. In this paper, we extend our studies of isotropic neutron IUGKS to encompass the transport equation with arbitrary anisotropic scattering. We first clarify the construction principle of IUGKS-PN scheme according to the general form of anisotropic scattering models. However, the construction of the scheme is complex and the versatility is not strong. To address these challenges, a more concise scheme IUGKS-AM is proposed based on the isotropic IUGKS framework, in which the higher-order moments of the neutron distribution function are estimated. We theoretically analyze the asymptotic property of IUGKS-AM, and verify the numerical performances in anisotropic model by numerical experiments. Finally, several complex anisotropic scattering models are computed by using the numerical scheme, demonstrating its general applicability. This study significantly enhances the practical utility of multi-scale neutron transport UGKS in engineering applications.

AMS subject classifications: 82D75, 76P05, 65M08

Key words: 3D neutron transport, UGKS, anisotropic scattering, time implicit.

1 Introduction

In previous works, we developed the unified gas kinetic scheme (UGKS) and the corresponding time-implicit scheme (IUGKS) for neutron transport simulations [1, 2]. The

*Corresponding author. *Email addresses:* tan_shuang@iapcm.ac.cn (S. Tan), sun_wenjun@iapcm.ac.cn (W. Sun), wei_junxia@iapcm.ac.cn (J. Wei)

results show that IUGKS achieves ideal accuracy and efficiency in the calculation of three-dimensional isotropic neutron transport equation, including the multi-group model calculations. In this paper, we further enhance the computational capabilities of IUGKS by extending it to accommodate anisotropic scattering models for practical applications. The transport equation form with general collision term is,

$$\begin{aligned}&\frac{1}{v(E)}\frac{\partial\phi(\mathbf{x},t,\mathbf{\Omega},E)}{\partial t}+\mathbf{\Omega}\cdot\nabla\phi(\mathbf{x},t,\mathbf{\Omega},E)+\Sigma(\mathbf{x},E)\phi(\mathbf{x},t,\mathbf{\Omega},E)\\&=\int\int\Sigma(\mathbf{x},E')f(E\to E',\mathbf{\Omega}\cdot\mathbf{\Omega}')\phi(\mathbf{x},t,\mathbf{\Omega}',E')\mathrm{d}E'\mathrm{d}\mathbf{\Omega}'+q(\mathbf{x},t,\mathbf{\Omega},E).\end{aligned}$$

Here the scattering phase function $f(\mathbf{x},\mathbf{\Omega}',E'\to\mathbf{\Omega},E)$ relys on the angle between $\mathbf{\Omega}$ and $\mathbf{\Omega}'$.

For single-scale SN methods, researches have been conducted on the computation of anisotropic equations [3]. The SN methods employ the splitting approach to deal with the convection and collision terms, and updates the transport equation by the source iteration method. By introducing the anisotropic scattering function directly into the collision term, the corresponding anisotropic numerical scheme can be constructed. The anisotropic collision term does not affect the calculation of the convection term, which is usually the core of numerical scheme construction. Despite the simple constructions, the SN schemes usually suffer from numerical stiffness issues. Therefore, the acceleration methods are needed to improve the convergence speed of the scheme. The common used acceleration methods include high-order/low-order (HOLO) [4], diffusion synthesis acceleration (DSA)/transport synthesis acceleration (TSA) [5,6], quasi-diffusion (QD), multi-grid method [7], etc. These methods have shown good performances in isotropic scattering simulations. But for the anisotropic models, due to that the scattering term has a significant effect on the spectral radius of the iterative equation, the acceleration method needs to be modified to maintain effective convergence. In practical three-dimensional high-order scattering models, these acceleration methods still present certain complexities and difficulties in the algorithms and code.

The mathematical properties of the neutron transport equation vary with the strength of the collision term. In the free transport region with weak collision, the equation is hyperbolic, while in the diffusion region with strong collision, the equation is parabolic. Therefore, transport is a typical multi-scale process. The corresponding numerical scheme should have asymptotic preserving (AP) properties. When the grid size or time step is fixed, and the Knudsen number approaches zero, a numerical scheme with AP properties can automatically recover the solution of the diffusion equation. This ensures the validity and accuracy of the scheme in a wide range of conditions. For isotropic scattering transport equation, the AP schemes have been widely studied [8–11]. Meanwhile, it is challenging to develop numerical schemes with AP properties for anisotropic scattering [12,13].

In recent years, UGKS has been widely studied in solving multi-scale equations. In UGKS, the cell-interface quantities and numerical fluxes are constructed with the time

evolution solution of the relaxation model, which naturally includes the evolution process from free transport to collision. The scheme was initially established to simulate the rarefied gas dynamics problems [14–16], and later extended to the linear dynamics model [17] and the calculation of radiation transport [18, 19]. In previous work, we developed the extended IUGKS [1, 2] for isotropic scattering neutron transport simulations. We have demonstrated that the scheme keeps AP properties at the transport to diffusion limit, and maintains ideal accuracy and convergence without other acceleration methods. Meanwhile, in recent years, the DUGKS developed by Guo et al. has also achieved success in the computation of multi-scale problems [20]. The construction idea of DUGKS is basically same as UGKS. The difference is that DUGKS reconstructs cell-interface quantities by integrating the relaxation model equation along the particle flight direction within a specific characteristic time/length scale. With this method, the single-step calculation cost can be reduced. DUGKS has also carried out relevant researches on the solution of steady neutron transport equation [21]. Song developed the scheme suitable for anisotropic scattering neutron transport models [22], in which the collision term is treated by source-iteration-like method, and the treatments for high-order moments are not considered.

Based on the introduction, extending the multi-scale UGKS to anisotropic scattering transport equations is an effective way to develop numerical schemes with good properties. The paper is organized as follows. Section 2 introduces the anisotropic scattering neutron transport equation. In section 3, the strict IUGKS-PN scheme for anisotropic scattering is introduced. Section 4 introduce the construction of the extended IUGKS-AM for arbitrary scattering models. Section 5 is numerical test. The conclusions are drawn in Section 6.

2 Neutron transport equation with anisotropic scattering

In physics, the distribution of neutrons in high-dimensional phase space $(\mathbf{x},t,\mathbf{\Omega},E)$ is described by neutron angular flux $\phi(\mathbf{x},t,\mathbf{\Omega},E)$. Here in addition to time t and space $\mathbf{x}$ variables, the neutron state also includes three degrees of freedom: microscopic motion angle $\mathbf{\Omega}$ and energy E. The governing equation for $\phi(\mathbf{x},t,\mathbf{\Omega},E)$ is,

$$\begin{aligned}&\frac{1}{v(E)}\frac{\partial\phi(\mathbf{x},t,\mathbf{\Omega},E)}{\partial t}+\mathbf{\Omega}\cdot\nabla\phi(\mathbf{x},t,\mathbf{\Omega},E)+\Sigma(\mathbf{x},E)\phi(\mathbf{x},t,\mathbf{\Omega},E)\\&=\int\int\Sigma(\mathbf{x},E')f(E'\to E,\mathbf{\Omega}\cdot\mathbf{\Omega}')\phi(\mathbf{x},t,\mathbf{\Omega}',E')\mathrm{d}E'\mathrm{d}\mathbf{\Omega}'+q(\mathbf{x},t,\mathbf{\Omega},E).\end{aligned}\tag{2.1}$$

In Eq. (2.1), $v(E)$ is neutron microscopic speed which is related to the energy E. $\Sigma(\mathbf{x},E)$ is the total cross section and $q(\mathbf{x},t,\mathbf{\Omega},E)$ is the external source term. $f(E\to E',\mathbf{\Omega}\cdot\mathbf{\Omega}')$ is the scattering phase function,

$$f(\mathbf{x},\mathbf{\Omega}',E'\to\mathbf{\Omega},E)=\sum_{l=0}^{L}\sum_{r=-l}^{l}f_l(\mathbf{x},E'\to E)Y_{lr}(\theta,\omega)Y_{lr}^*(\theta',\omega'),\tag{2.2}$$

where $Y_{lr}(\theta,\omega)$ is spherical harmonic function and $Y_{lr}^*(\theta,\omega)$ denotes the complex conjugate of $Y_{lr}(\theta,\omega)$.

In order to write Eq. (2.1) in a relaxation form, define the collision distribution as,

$$S(\mathbf{x},t,\mathbf{\Omega},E)=\int\int\frac{\Sigma(\mathbf{x},E')}{\Sigma(\mathbf{x},E)}f(E'\to E,\mathbf{\Omega}\cdot\mathbf{\Omega}')\phi(\mathbf{x},t,\mathbf{\Omega}',E')\mathrm{d}E'\mathrm{d}\mathbf{\Omega}'.$$

And further let the coefficient $\sigma_l(\mathbf{x},E'\to E)$ as,

$$\sigma_l(\mathbf{x},E'\to E)=\frac{\Sigma(\mathbf{x},E')}{\Sigma(\mathbf{x},E)}f_l(\mathbf{x},E'\to E).$$

Then the specific form of $S(\mathbf{x},t,\mathbf{\Omega},E)$ can be written as,

$$S(\mathbf{x},t,\mathbf{\Omega},E)=\sum_{l=0}^{L}\int\sigma_l(\mathbf{x},E'\to E)\sum_{r=-l}^{l}Y_{lr}(\theta,\omega)\varphi_l^r(\mathbf{x},t,E')\mathrm{d}E'. \tag{2.3}$$

Here $\varphi_l^r(\mathbf{x},t,E')$ is defined,

$$\varphi_l^r(\mathbf{x},t,E')=\int Y_{lr}^*(\theta,\omega)\phi(\mathbf{x},\mathbf{\Omega}',t,E')\mathrm{d}\mathbf{\Omega}'. \tag{2.4}$$

The specific expansion form of the collision term can be referenced in Appendix A. The neutron transport equation can be rearranged into the following form,

$$\frac{\partial\phi(\mathbf{x},t,\mathbf{\Omega},E)}{\partial t}+\boldsymbol{\xi}(E,\mathbf{\Omega})\cdot\nabla\phi(\mathbf{x},t,\mathbf{\Omega},E)=\frac{S(\mathbf{x},t,\mathbf{\Omega},E)-\phi(\mathbf{x},t,\mathbf{\Omega},E)}{\tau(\mathbf{x},E)}. \tag{2.5}$$

Here $\tau(\mathbf{x},E)=1/(v(E)\Sigma(\mathbf{x},E))$ is defined as the characteristic time, while $\boldsymbol{\xi}(E,\mathbf{\Omega})=v(E)\mathbf{\Omega}$ is the microscopic velocity of neutron motion.

3 IUGKS-PN scheme

For neutron transport, the energy spectrum usually spans multiple orders of magnitude. In the energy direction, the commonly used discretization is multi-group method. When the $\mathbf{\Omega}$-space is further discretized with the discrete ordinate method, the differential equation for the relaxed model (2.5) in the $(\mathbf{x},t)$-space is,

$$\frac{\partial\phi_{g,m}(\mathbf{x},t)}{\partial t}+\boldsymbol{\xi}_{g,m}\cdot\nabla\phi_{g,m}(\mathbf{x},t)=\frac{S_{g,m}(\mathbf{x},t)-\phi_{g,m}(\mathbf{x},t)}{\tau_g(\mathbf{x})}. \tag{3.1}$$

Here the subscript g represents the g-th discrete energy group, while the subscript m represents the m-th discrete ordinate directions of $\mathbf{\Omega}_m$. $\mathbf{\Omega}_m$ and the integral weight ω_m satisfy the following relations,

$$\sum_{m=1}^{M}\omega_m|\mathbf{\Omega}_m\cdot\mathbf{n}|^n=\begin{cases}0, & n\text{ is odd;}\\ \frac{4\pi}{n+1}, & n\text{ is even.}\end{cases}. \tag{3.2}$$

n is the direction unit vector. For the half-space integrals, it has,

$$\begin{aligned}\sum_{\mathbf{\Omega}_m\cdot\mathbf{n}>0}\omega_m|\mathbf{\Omega}_m\cdot\mathbf{n}|&=\pi,\\ \sum_{\mathbf{\Omega}_m\cdot\mathbf{n}>0}\omega_m|\mathbf{\Omega}_m\cdot\mathbf{n}|\mathbf{\Omega}_m&=\frac{2\pi}{3}\mathbf{n}.\end{aligned}\tag{3.3}$$

The discrete collision term is,

$$S_{g,m}(\mathbf{x},t)=\sum_{g'}\sum_{l=0}^{L}\sigma_{l,g'\to g}\sum_{r=-l}^{l}Y_{lr}(\theta_m,\omega_m)\varphi^r_{g',l}(\mathbf{x},t).$$

The relaxation equation (3.1) has the general solution,

$$\phi_{g,m}(\mathbf{x},t)=\phi_{0,g,m}(\mathbf{x}-\boldsymbol{\xi}_{g,m}(t-t_n))\mathrm{e}^{-(t-t_n)/\tau_g(\mathbf{x})}+\frac{1}{\tau_g(\mathbf{x})}\int_{t_n}^{t}S_{g,m}(\mathbf{x}',s)\mathrm{e}^{-(t-s)/\tau_g(\mathbf{x})}\mathrm{d}s.\tag{3.4}$$

$\mathbf{x}'=\mathbf{x}-\boldsymbol{\xi}_{g,m}(t-s)$ is the neutron trajectory in collision process. The solution describes the neutron physical evolution from free transport $\phi_{0,g,m}(\mathbf{x}-\boldsymbol{\xi}_{g,m}(t-t_n))$ to the collision state $S_{g,m}(\mathbf{x}',s)$.

The key point of the UGKS lies in constructing the cell-interface numerical flux $F_{g,m}(\mathbf{x})$ based on the multi-scale evolution solution (3.4). The flux can be expressed as

$$F_{g,m}(\mathbf{x})=\frac{1}{\Delta t}\int_{t_n}^{t_n+\Delta t}\oint\phi_{g,m}(\mathbf{x},t)\boldsymbol{\xi}_{g,m}\cdot\mathbf{n}\mathrm{d}s\mathrm{d}t.\tag{3.5}$$

To calculate the above numerical flux, we need to obtain the distribution functions of $\phi_{0,g,m}(\mathbf{x}-\boldsymbol{\xi}_{g,m}(t-t_n))$ and $S_{g,m}(\mathbf{x}',s)$.

The polynomial approximation of $\phi_{0,g,m}(\mathbf{x}-\boldsymbol{\xi}_{g,m}(t-t_n))$ is easy to be constructed with the solution of $\phi_{g,m}(\mathbf{x},t)$. Take the k-th boundary $\mathbf{s}_k$ as an example. Assume that the interface center is $\mathbf{x}_k$, and the outer normal direction is $\mathbf{n}_k$. The adjacent unit is labeled as j. In order to obtain a second order scheme, the linear distribution of $\phi_{0,g,m}(\mathbf{x},t)$ around the cell-interface $\mathbf{s}_k$ is constructed as,

$$\phi_{0,g,m}=\phi^l_{g,m}\mathrm{H}[\dot{\Omega}_{m,k}]+\phi^r_{g,m}\mathrm{H}[-\dot{\Omega}_{m,k}].$$

Here $\dot{\Omega}_{m,k}$ is $\mathbf{\Omega}_m\cdot\mathbf{n}_k$, and $\mathrm{H}[\cdot]$ is the Heaviside function. The linear function of ϕ on the left and right sides of the interface is,

$$\begin{cases}\phi^l_{g,m}=\phi^L_{g,m,k}+\nabla\phi_{g,m,i}\cdot(\mathbf{x}-\mathbf{x}_k), & (\mathbf{x}-\mathbf{x}_k)\cdot\mathbf{n}_k<0,\\ \phi^r_{g,m}=\phi^R_{g,m,k}+\nabla\phi_{g,m,j}\cdot(\mathbf{x}-\mathbf{x}_k), & (\mathbf{x}-\mathbf{x}_k)\cdot\mathbf{n}_k>0.\end{cases}$$

$\phi^L_{g,m}$ and $\phi^R_{g,m}$ are the values on the left and right cells of the interface. $\nabla\phi_{g,m,i}$ and $\nabla\phi_{g,m,j}$ are the slopes within the corresponding cell. With the cell centroid $\mathbf{x}_i$ and $\mathbf{x}_j$ and the

center quantity $\phi_{g,m,i}$ and $\phi_{g,m,j}$, we can easily get that,

$$\begin{cases} \phi^L_{g,m,k}=\phi_{g,m,i}+\nabla\phi_{g,m,i}\cdot(\mathbf{x}_k-\mathbf{x}_i), \\ \phi^R_{g,m,k}=\phi_{g,m,j}+\nabla\phi_{g,m,j}\cdot(\mathbf{x}_k-\mathbf{x}_j). \end{cases}$$

Without loss of generality, assume $\mathbf{x}_k=0$ and $t_n=0$, the polynomial form of $\phi_{g,m}(\mathbf{x}_k-\boldsymbol{\xi}_{g,m}(t-t_n))$ can be obtained,

$$\begin{aligned}\phi_{g,m}(\mathbf{x}_k-\boldsymbol{\xi}_{g,m}(t-t_n))=&\left(\phi^L_{g,m,k}-\nabla\phi_{g,m,i}\cdot\boldsymbol{\xi}_{g,m}t)\right)\mathrm{H}[\,\dot{\Omega}_{m,k}], \\ &+\left(\phi^R_{g,m,k}-\nabla\phi_{g,m,j}\cdot\boldsymbol{\xi}_{g,m}t)\right)\mathrm{H}[-\dot{\Omega}_{m,k}].\end{aligned} \tag{3.6}$$

Similarly, the linear approximation of $S_{g,m}(\mathbf{x}',s)$ is,

$$\begin{aligned}S_{g,m}(\mathbf{x}',s)=&\left(S^L_{g,m,k}-\nabla S_{g,m,i}\cdot\boldsymbol{\xi}_{g,m}(t-s))\right)\mathrm{H}[\,\dot{\Omega}_{m,k}] \\ &+\left(S^R_{g,m,k}-\nabla S_{g,m,j}\cdot\boldsymbol{\xi}_{g,m}(t-s))\right)\mathrm{H}[-\dot{\Omega}_{m,k}],\end{aligned} \tag{3.7}$$

where the $S^L_{g,m,k}$ and $S^R_{g,m,k}$ are,

$$\begin{cases} S^L_{g,m,k}=S_{g,m,i}-\nabla S_{g,m,i}\cdot\mathbf{x}_i; \\ S^R_{g,m,k}=S_{g,m,j}-\nabla S_{g,m,j}\cdot\mathbf{x}_j. \end{cases}$$

Here we omit the time derivative term $\nabla_t S_{g,m,k}$. As demonstrated in subsequent analysis and tests, this simplification shows no adverse impact on the AP property or temporal accuracy of the scheme.

3.1 IUGKS-P0 for isotropic model

Before dealing with the anisotropic scattering case, the implicit unified gas kinetic scheme (IUGKS) for isotropic scattering models is overviewed in this subsection. According to the derivation in Appendix A, the isotropic collision distribution is,

$$S_g(\mathbf{x},t)=\frac{1}{4\pi}\sum_{g'}\sigma_{0,g'\to g}(\mathbf{x})\varphi_{g'}(\mathbf{x},t).$$

$\varphi_{g'}(\mathbf{x},t)$ is the 0-th moment of ϕ,

$$\varphi_{g'}(\mathbf{x},t)=\int\phi_{g'}(\mathbf{x},t,\boldsymbol{\Omega})\mathrm{d}\boldsymbol{\Omega},$$

where the superscript (0) is omitted for simplify writing. After substituting $S_g(\mathbf{x},t)$ into Eqs. (3.7) and (3.5), the numerical flux is,

$$\begin{aligned}F_{g,m,k}=&T^3_{g,k}\dot{\xi}_{g,m,k}\left(\phi^L_{g,m,k}\mathrm{H}[\dot{\Omega}_{m,k}]+\phi^R_{g,m,k}\mathrm{H}[-\dot{\Omega}_{m,k}]\right)\\&-T^4_{g,k}\dot{\xi}^2_{g,m,k}\left(\nabla\phi_{g,m,i}\cdot\mathbf{n}_k\mathrm{H}[\dot{\Omega}_{m,k}]+\nabla\phi_{g,m,j}\cdot\mathbf{n}_k\mathrm{H}[-\dot{\Omega}_{m,k}]\right)\\&+T^1_{g,k}\dot{\xi}_{g,m,k}\sum_{g'}\frac{\sigma_{0,g'\to g,k}}{4\pi}\left(\varphi^L_{g',k}\mathrm{H}[\dot{\Omega}_{m,k}]+\varphi^R_{g',k}\mathrm{H}[-\dot{\Omega}_{m,k}]\right)\\&+T^2_{g,k}\dot{\xi}^2_{g,m,k}\sum_{g'}\frac{\sigma_{0,g'\to g,k}}{4\pi}\left(\nabla\varphi_{g',i}\cdot\mathbf{n}_k\mathrm{H}[\dot{\Omega}_{m,k}]+\nabla\varphi_{g',j}\cdot\mathbf{n}_k\mathrm{H}[-\dot{\Omega}_{m,k}]\right).\end{aligned}\tag{3.8}$$

The normal velocity of the interface is $\dot{\xi}_{g,m,k}=\boldsymbol{\xi}_{g,m}\cdot\mathbf{n}_k$ which can also be calculated as $v_g\dot{\Omega}_{m,k}$. $T^{(*)}_{g,k}$ are the time-space integral terms,

$$\begin{aligned}T^3_{g,k}&=\frac{\tau_g}{\Delta t}(1-\mathrm{e}^{-\Delta t/\tau_g})\oint\mathrm{d}s_k,\\T^4_{g,k}&=\left(-\tau_g\mathrm{e}^{-\Delta t/\tau_g}+\tau_gT^3_{g,k}\right)\oint\mathrm{d}s_k,\\T^1_{g,k}&=\left(1-T^3_{g,k}\right)\oint\mathrm{d}s_k,\\T^2_{g,k}&=\left(-\tau_gT^1_{g,k}+T^4_{g,k}\right)\oint\mathrm{d}s_k.\end{aligned}\tag{3.9}$$

According to the stability analysis in Appendix B, the time step Δt for the flux evolution in Eq. (3.8) should satisfy the stability condition,

$$\Delta t=\min\left(\frac{\Delta_i}{v_g},\frac{3\Sigma_{g,i}\Delta_i^2}{2v_g}\right).\tag{3.10}$$

Here $\Delta_i=\min(\Delta x_{1,i},\Delta x_{2,i},\Delta x_{3,i})$ is the grid scale of i-th cell. From Eq. (3.8), we should obtain the solution of $\varphi_g(\mathbf{x},t)$ to close the calculation of $F^{\phi}_{g,m,k}$. This is the particular part of UGKS that is different from the commonly used single-scale SN scheme.

By integrating Eq. (3.1) in the $\boldsymbol{\Omega}$ direction, one can get the governing equations of $\varphi_g(\mathbf{x},t)$,

$$\frac{\partial\varphi_g(\mathbf{x},t)}{\partial t}+\sum_m\omega_m\left(\boldsymbol{\xi}_{g,m}\cdot\nabla\phi_{g,m}(\mathbf{x},t)\right)=\frac{S_g(\mathbf{x},t)-\varphi_g(\mathbf{x},t)}{\tau_g(\mathbf{x})}.\tag{3.11}$$

Accordingly, the numerical flux of $\varphi_g(\mathbf{x},t)$ can be calculated as,

$$\mathcal{F}_g=\sum\omega_mF_{g,m}(\mathbf{x}).$$

With $F^{\phi}_{g,m}(\mathbf{x})$ in Eq. (3.8) and the properties of discrete ordinates in Eqs. (3.2) and (3.3), $\mathcal{F}_g$

can be organized as,

$$\begin{aligned}\mathcal{F}_{g,k}=&T^3_{g,k}\sum\omega_m\dot{\xi}_{g,m,k}\left(\phi^L_{g,m,k}\mathrm{H}[\dot{\Omega}_{m,k}]+\phi^R_{g,m,k}\mathrm{H}[-\dot{\Omega}_{m,k}]\right)\\&-T^4_{g,k}\sum\omega_m\dot{\xi}^2_{g,m,k}\left(\nabla\phi_{g,m,i}\cdot\mathbf{n}_k\mathrm{H}[\dot{\Omega}_{m,k}]+\nabla\phi_{g,m,j}\cdot\mathbf{n}_k\mathrm{H}[-\dot{\Omega}_{m,k}]\right)\\&+T^1_{g,k}v_g\sum_{g'}\sigma_{0,g'\to g,k}\frac{\varphi^L_{g',k}-\varphi^R_{g',k}}{4}\\&+T^2_{g,k}v_g^2\sum_{g'}\sigma_{0,g'\to g,k}\frac{\nabla\varphi_{g',i}\cdot\mathbf{n}_k+\nabla\varphi_{g',j}\cdot\mathbf{n}_k}{6}.\end{aligned}\tag{3.12}$$

For Eqs. (3.1) and (3.11), finite volume method is used in the spatial discretization, and time-implicit discretization is used in the temporal direction. We obtain the fully discrete form of the macro auxiliary equation firstly,

$$\begin{aligned}&\left[\frac{1}{\Delta t_P}+\epsilon'\frac{1-\sigma_{0,g,i}}{\tau_{g,i}}+\sum_k\mathcal{A}^+_{g,k}\right]\Delta\varphi^p_{g,i}+\sum_k\mathcal{A}^-_{g,k}\Delta\varphi^p_{g,j}\\=&-\epsilon'\sum_k\mathcal{F}^p_{g,k}+\frac{\epsilon'}{\tau_{g,i}}\left(\mathcal{S}^p_{g,i}-\varphi^p_{g,i}\right)-\epsilon\sum_k\mathcal{F}^n_{g,k}+\frac{\epsilon}{\tau_{g,i}}\left(\mathcal{S}^n_{g,i}-\varphi^n_{g,i}\right)-\frac{1}{\Delta t_P}\left(\varphi^p_{g,i}-\varphi^n_{g,i}\right).\end{aligned}\tag{3.13}$$

Δt_P is the physical time step, which is determined according to the time scale of the specific physical process. $\Delta\varphi^p_{g,i}=\varphi^{p+1}_{g,i}-\varphi^p_{g,i}$ is the residual at the cell i, while p is the iteration number. $\sigma_{0,g,i}$ is short for $\sigma_{0,g\to g,i}$. With different values of ϵ (where $\epsilon'=1-\epsilon$), Eq. (3.13) represents different implicit time schemes uniformly, which are the 1st-order backward Euler (B-E) scheme ($\epsilon=0$) and the 2nd-order Crank-Nicolson (C-N) scheme ($\epsilon=0.5$). $\mathcal{S}_g(\mathbf{x},t)$ is the angular integral of generalized equilibrium state $S_g(\mathbf{x},t)$,

$$\mathcal{S}^p_{g,i}=\sum_{g'}\sigma_{0,g'\to g,i}\varphi^p_{g',i}.$$

The approximate flux Jacobian coefficients $\mathcal{A}^\pm_{g,k}$ are,

$$\begin{aligned}\mathcal{A}^+_{g,k}&=\frac{\epsilon'}{V_i}\left(T^3_{g,k}\frac{\sum\omega_m\dot{\xi}_{g,m,k}\phi^p_{g,m,i}\mathrm{H}[\,\dot{\Omega}_{m,k}]}{\varphi^p_{g,i}}+T^2_{g,k}\frac{v_g^2\sigma_{0,g,k}}{3\Delta_{ij}}\right),\\\mathcal{A}^-_{g,k}&=\frac{\epsilon'}{V_i}\left(T^3_{g,k}\frac{\sum\omega_m\dot{\xi}_{g,m,k}\phi^p_{g,m,j}\mathrm{H}[-\dot{\Omega}_{m,k}]}{\varphi^p_{g,j}}+T^2_{g,k}\frac{v_g^2\sigma_{0,g,k}}{3\Delta_{ji}}\right),\end{aligned}$$

where

$$\Delta_{ij}=\mathbf{x}_i\cdot\mathbf{n}_k-\mathbf{x}_j\cdot\mathbf{n}_k,\quad\Delta_{ji}=\mathbf{x}_j\cdot\mathbf{n}_k-\mathbf{x}_i\cdot\mathbf{n}_k.$$

In the construction of macroscopic flux Jacobian, it is assumed that $\varphi_g$is continuous and smooth at the cell interfaces.

The fully implicit discrete form of microscopic transport equation (3.1) is,

$$\begin{aligned}&\left[\frac{1}{\Delta t_p}+\frac{\epsilon'}{\tau}+\sum_k A^+_{g,m,k}\right]\Delta\phi^p_{g,m,i}+\sum_k A^-_{g,m,k}\Delta\phi^p_{g,m,j}\\ =&-\epsilon'\sum_k F^{\phi,p}_{g,m,k}+\frac{\epsilon'}{\tau_{g,i}}\left(S^{p+1}_{g,i}-\phi^p_{g,m,i}\right)\\ &-\epsilon\sum_k F^{\phi,n}_{g,m,k}+\frac{\epsilon}{\tau_{g,i}}\left(S^n_{g,i}-\phi^n_{g,m,i}\right)-\frac{1}{\Delta t_p}\left(\phi^p_{g,m,i}-\phi^n_{g,m,i}\right).\end{aligned}\tag{3.14}$$

$\Delta\phi^p_{g,m,i}=\phi^{p+1}_{g,m,i}-\phi^p_{g,m,i}$ is the residual for $\phi_{g,m,i}$ at the cell i. The scheme coefficients $A^\pm_{g,k}$ are,

$$A^\pm_{g,k}=\epsilon'\dot{\xi}_{g,m,k}\mathrm{H}[\pm\dot{\Omega}_{m,k}].$$

The linear systems in Eqs. (3.13) and (3.14) can be solved with the Lower-Upper Symmetric Gauss-Seidel (LU-SGS) method [23]. The discrete expression of IUGKS-P0 is exactly the form of IUGKS in general grid, while the detailed derivations can be referred in Tan [2]. Since it is a routine procedure, it will not be elaborated upon in this article.

To sum up, the calculation flowchart of IUGKS-P0 for neutron transport equation with isotropic scattering is as shown in Algorithm 1.

Algorithm 1: IUGKS-P0 for isotropic scattering neutron transport

1. Construct the evolution solution (3.4) with $\phi_{g,m}$ and $S_{g,m}$;
2. Calculate macro flux (3.12) and solve the auxiliary equation (3.13) to get φ_g;
3. Update S_g with φ_g and substitute into micro flux equation (3.8);
4. Solve the micro transport equation (3.14) to get $\phi_{g,m}$;
5. Update φ_g and S_g with $\phi_{g,m}$, and goto the next loop.

3.2 IUGKS-PN for anisotropic model

When considering the anisotropic scattering models, if the collision distribution $S_{g,m}(\mathbf{x},t)$ is given in Eq. (2.3), the above IUGKS-P0 for isotropic scattering neutron transport can be extended directly.

According to the analysis in Appendix A, the evolution solution is related with all the r-th ($r\leq L$) order moments of ϕ for the L-th order anisotropic scattering model. Define the r-th order moments of ϕ as,

$$\varphi^{(r1,r2,r3)}(\mathbf{x},t,E)=\int\Omega_1^{r_1}\Omega_2^{r_2}\Omega_3^{r_3}\phi(\mathbf{x},t,\mathbf{\Omega},E)\mathrm{d}\Omega,\quad r_1+r_2+r_3=r.$$

Therefore, in order to close the construction of Eq. (3.4), the equations of $\varphi^{(r1,r2,r3)}(\mathbf{x},t,E)$ need to be solved,

$$\frac{\partial \varphi^{(r1,r2,r3)}(\mathbf{x},t,E)}{\partial t}+\nabla\cdot\left(\int \boldsymbol{\xi}(E)\Omega_1^{r_1}\Omega_2^{r_2}\Omega_3^{r_3}\phi_g(\mathbf{x},t,\boldsymbol{\Omega})\mathrm{d}\Omega\right)$$
$$=\frac{\int \Omega_1^{r_1}\Omega_2^{r_2}\Omega_3^{r_3}S_g(\mathbf{x},t,\boldsymbol{\Omega})\mathrm{d}\Omega-\varphi^{(r1,r2,r3)}(\mathbf{x},t,E)}{\tau_g(\mathbf{x})}. \tag{3.15}$$

The numerical flux of $\varphi_d^{(r1,r2,r3)}(\mathbf{x},t,E)$ can be get similarly,

$$\mathcal{F}_{g,k}^{(r1,r2,r3)}=\frac{1}{\Delta t}\int\int_{t_n}^{t_n+\Delta t}\oint \boldsymbol{\xi}_g\cdot\mathbf{n}_k\Omega_1^{r_1}\Omega_2^{r_2}\Omega_3^{r_3}\phi_{g,k}(t,\boldsymbol{\Omega})\mathrm{d}s_k\mathrm{d}t\mathrm{d}\Omega.$$

Therefore, the solution of IUGKS-PN for neutron transport with PN scattering model of Eq. (2.3) should be modified as Algorithm 2.

Algorithm 2: IUGKS-PN for PN scattering neutron transport

1. Construct evolution solution (3.4) with initial $\phi_{g,m}$ and $S_{g,m}$;
2. Calculate macro flux (3.12) and solve the auxiliary equation (3.13) to get φ_g;
3. For $r=1,L$; For $r_1+r_2+r_3=r$;
   Calculate the flux $\mathcal{F}_{g,k}^{(r1,r2,r3)}$ and solve the auxiliary equation sets of $\varphi_g^{(r1,r2,r3)}$ in (3.15);
4. Calculate $S_{g,m}$ with $\varphi_g^{(r1,r2,r3)}$ and substitute into micro flux equation (3.8) ;
5. Solve the micro transport equation (3.14) to get $\phi_{g,m}$;
6. Update $\varphi_g^{(r1,r2,r3)}$ and $S_{g,m}$ with $\phi_{g,m}$, and goto the next loop.

According to Algorithm 2, it is easy to see that the construction of IUGKS-PN is closely related to the specific expression of the phase function $f(\mathbf{x},\boldsymbol{\Omega}',E'\to\boldsymbol{\Omega},E)$. As in step 3, the number of auxiliary equations is changing with different L. Especially in three-dimensional multi-group computations, $G\sum_{r=0}^{L}\frac{(r+2)(r+1)}{2}$ additional auxiliary equations need to be solved for the L-th order moment term. Therefore, IUGKS-PN is not only complex in scheme construction, but also has poor universality.

4 IUGKS with anisotropic-scattering modification

To avoid introducing additional auxiliary macro equations as IUGKS-PN, a more general numerical scheme for arbitrary anisotropic scattering model equations is developed in this section. We also conducted a detailed analysis of the AP characteristics for the scheme.

Assume the discrete form of neutron flux $\phi(\mathbf{x},t,\boldsymbol{\Omega},E)$ can be decomposed into the following forms,

$$\phi(\mathbf{x},t,\boldsymbol{\Omega},E)=\varphi(\mathbf{x},t,E)h(\mathbf{x},t,\boldsymbol{\Omega},E). \tag{4.1}$$

$h(\mathbf{x},t,\mathbf{\Omega},E)$ is a normalized function which characterizes the shape distribution of the neutron flux ϕ with energy E at the space-time point $(\mathbf{x},t)$ in angular space $\mathbf{\Omega}$.

As mentioned before, the key to the construction of neutron transport UGKS lies in the calculation or approximation of the collision term $S(\mathbf{x},t,\mathbf{\Omega},E)$. Define the anisotropic scattering integral of the function $h(\mathbf{x},t,\mathbf{\Omega},E)$ as,

$$\varsigma(\mathbf{x},t,\mathbf{\Omega},E'\to E)=\frac{\Sigma(\mathbf{x},E')}{\Sigma(\mathbf{x},E)}\int f(E'\to E,\mathbf{\Omega}\cdot\mathbf{\Omega}')h(\mathbf{x},t,\mathbf{\Omega}',E')\mathrm{d}\mathbf{\Omega}'.$$

Then the collision distribution $S_g(\mathbf{x},\mathbf{\Omega})$ can be simplified as,

$$S(\mathbf{x},t,\mathbf{\Omega},E)=\int\varphi(\mathbf{x},t,E')\varsigma(\mathbf{x},t,\mathbf{\Omega},E'\to E)\mathrm{d}E'. \tag{4.2}$$

When $f(E'\to E,\mathbf{\Omega}\cdot\mathbf{\Omega}')$ is defined as Eq. (2.2), the corresponding expression of $\varsigma(\mathbf{x},t,\mathbf{\Omega},E'\to E)$ is,

$$\varsigma_{g'\to g}(\mathbf{x},t,\mathbf{\Omega})=\frac{\Sigma_{g'}(\mathbf{x})}{\Sigma_g(\mathbf{x})}\sum_{l=0}^{L}f_{l,g'\to g}(\mathbf{x})\sum_{r=-l}^{l}Y_{lr}(\theta,\omega)\Pi^r_{g',l}(\mathbf{x},t). \tag{4.3}$$

Here $\Pi^r_{g,l}(\mathbf{x},t)$ is the moment of $h(\mathbf{x},t,\mathbf{\Omega},E)$,

$$\Pi^r_{g,l}(\mathbf{x},t)=\int Y^*_{lr}(\theta,\omega)h_g(\mathbf{x},t,\mathbf{\Omega})\mathrm{d}\mathbf{\Omega}.$$

It can be seen that, when $h_g(\mathbf{x},t,\mathbf{\Omega})$ is known, the anisotropic scattering collision distribution function $S_g(\mathbf{x},\mathbf{\Omega})$ is only related with the 0-th order moment $\varphi_{g'}(\mathbf{x},t)$. Thus, in order to obtain the modified scheme only related to $\varphi_{g'}(\mathbf{x},t)$, the distribution of $h_g(\mathbf{x},t,\mathbf{\Omega})$ will be get by predictor-corrector method.

In this paper, we approximate the angular distribution of ϕ for current $p+1$-th iteration by using the shape function of the p-th iteration step. This means that the evolution of the angular direction is explicitly handled,

$$h^*_g(\mathbf{x},\mathbf{\Omega})=\frac{\phi^p_g(\mathbf{x},\mathbf{\Omega})}{\varphi^p_g(\mathbf{x})}. \tag{4.4}$$

The premise for this assumption to be correct is that the neutron flux converges in the $\mathbf{\Omega}$ direction. Since the neutron flux is positive in general, the prediction in (4.4) is nonsingular. With $h^*_g(\mathbf{x},\mathbf{\Omega})$ in hand, we only need to solve the governing equations of $\phi_g(\mathbf{x},t,\mathbf{\Omega})$ and $\varphi_g(\mathbf{x},t)$ to close the evolution solution in Eq. (3.4) for any arbitrary anisotropic scattering models. The scheme construction is basically same with the isotropic IUGKS-P0. Thus we refer to this algorithm as IUGKS with anisotropic modification (IUGKS-AM) in this paper. Furthermore, it can be get that IUGKS-P0 is actually a special form of IUGKS-AM with $h_g(\mathbf{x},t,\mathbf{\Omega})\equiv 1$.

According to Algorithm 1, the details of Steps 2-5 in IUGKS-AM discretization are emphasized in following. It should be pointed out here that the approximation used in Eq. (4.4) should have influences on the numerical scheme. We will analyze and verify this both theoretically and numerically in the following AP property analysis and numerical testing in the next section.

4.1 Construction of IUGKS-AM

The governing equation for $\varphi_g(\mathbf{x})$ in IUGKS-AM is,

$$\frac{\partial \varphi_g(\mathbf{x},t)}{\partial t}+\int \boldsymbol{\xi}_g\cdot\nabla\phi_g(\mathbf{x},t,\boldsymbol{\Omega})\mathrm{d}\Omega=\frac{\tilde{\mathcal{S}}_g(\mathbf{x},t)-\varphi_g(\mathbf{x},t)}{\tau_g(\mathbf{x})}. \tag{4.5}$$

With Eq. (4.2), the integral of collision term $S(\mathbf{x},t,\boldsymbol{\Omega},E)$ is,

$$\tilde{\mathcal{S}}_g(\mathbf{x},t)=\sum_{g'}\varphi_{g'}(\mathbf{x},t)\int \varsigma_{g'\to g}(\mathbf{x},t,\boldsymbol{\Omega})\mathrm{d}\boldsymbol{\Omega}.$$

Applying Eq. (4.1) to the micro numerical flux equation (3.8), and integrating in $\boldsymbol{\Omega}$ direction, the cell-interface numerical flux for φ_g in IUGKS-AM can be obtained as,

$$\begin{aligned}\tilde{\mathcal{F}}^p_{g,k}=&T^3_{g,k}\left[\mathcal{H}^{1,+}_{g,i,k}\varphi^{p,L}_{g,k}+\mathcal{H}^{1,-}_{g,j,k}\varphi^{p,R}_{g,k}\right]\\&-T^4_{g,k}\left(\mathcal{H}^{2,+}_{g,i,k}\nabla\varphi^p_{g,i}\cdot\mathbf{n}_k+\mathcal{H}^{2,-}_{g,j,k}\nabla\varphi^p_{g,j}\cdot\mathbf{n}_k\right)\\&+T^1_{g,k}\sum_{g'}\left(\mathcal{G}^{1,+}_{g'\to g,i,k}\varphi^{p,L}_{g',k}+\mathcal{G}^{1,-}_{g'\to g,j,k}\varphi^{p,R}_{g',k}\right)\\&+T^2_{g,k}\sum_{g'}\left(\mathcal{G}^{2,+}_{g'\to g,i,k}\nabla\varphi^p_{g',i}\cdot\mathbf{n}_k+\mathcal{G}^{2,-}_{g'\to g,j,k}\nabla\varphi^p_{g',j}\cdot\mathbf{n}_k\right).\end{aligned}$$

The half space integral of r-th moment for the shape function $h^*_{g,i}(\boldsymbol{\Omega})$ is defined as,

$$\begin{aligned}\mathcal{H}^{r,\pm}_{g,i,k}&=v^r_g\int\dot{\Omega}^r_k h^*_{g,i}(\Omega)\mathrm{H}[\pm\dot{\Omega}_k]\mathrm{d}\Omega,\\ \mathcal{G}^{r,\pm}_{g'\to g,i,k}&=v^r_g\int\dot{\Omega}^r_k \varsigma^*_{g'\to g,i}(\Omega)\mathrm{H}[\pm\dot{\Omega}_k]\mathrm{d}\Omega,\end{aligned}$$

where $\dot{\Omega}_k=\boldsymbol{\Omega}\cdot\mathbf{n}_k$.

The fully discrete form of Eq. (4.5) can be deduced,

$$\begin{aligned}&\left[\frac{1}{\Delta t_P}+\epsilon'\frac{1-\tilde{\sigma}_{0,g,i}}{\tau_{g,i}}+\sum_k\tilde{\mathcal{A}}^+_{g,k}\right]\Delta\varphi^p_{g,i}+\sum_k\tilde{\mathcal{A}}^-_{g,k}\Delta\varphi^p_{g,j}\\&=-\epsilon'\sum_k\tilde{\mathcal{F}}^p_{g,k}+\frac{\epsilon'}{\tau_{g,i}}\left(\tilde{\mathcal{S}}^p_{g,i}-\varphi^p_{g,i}\right)-\epsilon\sum_k\tilde{\mathcal{F}}^n_{g,k}+\frac{\epsilon'}{\tau_{g,i}}\left(\tilde{\mathcal{S}}^n_{g,i}-\varphi^n_{g,i}\right)-\frac{1}{\Delta t_P}\left(\varphi^p_{g,i}-\varphi^n_{g,i}\right).\end{aligned} \tag{4.6}$$

Here

$$\tilde{\sigma}_{0,g,i}=\int \varsigma_{g\to g}(\mathbf{x},t,\mathbf{\Omega})\mathrm{d}\mathbf{\Omega},$$

and the coefficients $\tilde{\mathcal{A}}^{\pm}_{g,k}$ are,

$$\tilde{\mathcal{A}}^{+}_{g,k}=\frac{\epsilon'}{V_i}\left(T^3_{g,k}\mathcal{H}^{1,+}_{g,i,k}+T^1_{g,k}\mathcal{G}^{1,+}_{g,i,k}+\frac{1}{\Delta_{ij}}T^2_{g,k}\mathcal{G}^{2,+}_{g,i,k}\right),$$
$$\tilde{\mathcal{A}}^{-}_{g,k}=\frac{\epsilon'}{V_i}\left(T^3_{g,k}\mathcal{H}^{1,-}_{g,j,k}+T^1_{g,k}\mathcal{G}^{1,-}_{g,j,k}+\frac{1}{\Delta_{ji}}T^2_{g,k}\mathcal{G}^{2,-}_{g,j,k}\right).$$

After Solving the linear system of (4.6), we can update $\varphi^{p+1}(\mathbf{x},t,E)=\varphi^{p}(\mathbf{x},t,E)+\Delta\varphi^{p}_{g,i}$, so that the collision distribution for $p+1$ iteration can be predicted as,

$$\tilde{S}^{p+1}_{g,m,i}=\sum_{g'}\varsigma^{*}_{g'\to g,m,i}\varphi^{p+1}_{g',i}. \tag{4.7}$$

Then the discretization of the microscopic transport equation in IUGKS-AM has the same expression as Eq. (3.14),

$$\begin{aligned}&\left[\frac{1}{\Delta t_P}+\frac{\epsilon'}{\tau}+\sum_k A^{+}_{g,m,k}\right]\Delta\phi^{p}_{g,m,i}+\sum_k A^{-}_{g,m,k}\Delta\phi^{p}_{g,m,j}\\ =&-\epsilon'\sum_k\tilde{F}^{p}_{g,m,k}+\frac{\epsilon'}{\tau_{g,i}}\left(\tilde{S}^{p+1}_{g,m,i}-\phi^{p}_{g,m,i}\right)\\ &-\epsilon\sum_k\tilde{F}^{n}_{g,m,k}+\frac{\epsilon}{\tau_{g,i}}\left(\tilde{S}^{n}_{g,m,i}-\phi^{n}_{g,m,i}\right)-\frac{1}{\Delta t_P}\left(\phi^{p}_{g,m,i}-\phi^{n}_{g,m,i}\right).\end{aligned} \tag{4.8}$$

In Eq. (4.8), the numerical flux is,

$$\begin{aligned}\tilde{F}^{p}_{g,m,k}=&T^3_{g,k}\dot{\xi}_{g,m,k}\left(\phi^{p,L}_{g,m,k}\mathrm{H}[\dot{\Omega}_{m,k}]+\phi^{p,R}_{g,m,k}\mathrm{H}[-\dot{\Omega}_{m,k}]\right)\\ &-T^4_{g,k}\dot{\xi}^2_{g,m,k}\left(\nabla\phi^{p}_{g,m,i}\cdot\mathbf{n}_k\mathrm{H}[\dot{\Omega}_{m,k}]+\nabla\phi^{p}_{g,m,j}\cdot\mathbf{n}_k\mathrm{H}[-\dot{\Omega}_{m,k}]\right)\\ &+T^1_{g,k}\dot{\xi}_{g,m,k}\left(\tilde{S}^{p+1,L}_{g,m,k}\mathrm{H}[\dot{\Omega}_{m,k}]+\tilde{S}^{p+1,R}_{g,m,k}\mathrm{H}[-\dot{\Omega}_{m,k}]\right)\\ &+T^2_{g,k}\dot{\xi}^2_{g,m,k}\left(\nabla\tilde{S}^{p+1}_{g,m,i}\cdot\mathbf{n}_k\mathrm{H}[\dot{\Omega}_{m,k}]+\nabla\tilde{S}^{p+1}_{g,m,j}\cdot\mathbf{n}_k\mathrm{H}[-\dot{\Omega}_{m,k}]\right).\end{aligned} \tag{4.9}$$

Again, solving the linear system of (4.8) and updating $\phi^{p+1}_{g}(\mathbf{x},t,\mathbf{\Omega})$, we complete one iteration of the numerical scheme. Update the shape function as,

$$h^{*}_{g}(\mathbf{x},\mathbf{\Omega})=\frac{\phi^{p+1}_{g}(\mathbf{x},\mathbf{\Omega})}{\varphi^{p+1}_{g}(\mathbf{x})}. \tag{4.10}$$

The calculation process will enter the next iterative loop if it is not convergent.

It can be seen from the discretization process of IUGKS-AM, once introducing $h(\mathbf{x},t,\mathbf{\Omega},E)$ and $\varsigma(\mathbf{x},t,\mathbf{\Omega},E'\to E)$ in $S(\mathbf{x},t,\mathbf{\Omega},E)$, there need not impose additional constraints on the form of scattering term. Therefore, IUGKS-AM can be applied to any anisotropic scattering model, even if the scattering terms can not be expressed by spherical harmonic function.

4.2 Asymptotic-preserving analysis

The AP property of IUGKS-AM under free transport limit is obvious. In this subsection, we mainly analyze the scheme AP property in diffusion limit.

In neutron transport, the Kn number which describe the relative scale of grid size and neutron mean free path is defined as $\mathrm{Kn}(E)=1/\Delta\Sigma(\mathbf{x},E)$, which is $\mathrm{Kn}_g\propto\tau_g/\Delta t$. In the diffusion limit when $\mathrm{Kn}_g\ll 1$, the time integral terms in Eq. (3.9) has the limit values,

$$\lim_{\mathrm{Kn}_g\ll 1} T^3_{g,k}=0,\quad \lim_{\mathrm{Kn}_g\ll 1} T^4_{g,k}=0,\quad \lim_{\mathrm{Kn}_g\ll 1} T^1_{g,k}=\oint \mathrm{d}s_k,\quad \lim_{\mathrm{Kn}_g\ll 1} T^2_{g,k}=-\tau_g\oint \mathrm{d}s_k.$$

Then as $\mathrm{Kn}_g\ll 1$, the numerical flux in Eq. (4.9) can be simplified as,

$$\begin{aligned}\tilde{F}_{g,m,k}=&\Big[\dot{\xi}_{g,m,k}\Big(\tilde{S}^{*,L}_{g,m,k}\mathrm{H}[\dot{\Omega}_{m,k}]+\tilde{S}^{*,R}_{g,m,k}\mathrm{H}[-\dot{\Omega}_{m,k}]\Big)\\&-\tau_g\dot{\xi}^2_{g,m,k}\Big(\nabla\tilde{S}^{*}_{g,m,i}\cdot\mathbf{n}_k\mathrm{H}[\dot{\Omega}_{m,k}]+\nabla\tilde{S}^{*}_{g,m,j}\cdot\mathbf{n}_k\mathrm{H}[-\dot{\Omega}_{m,k}]\Big)\Big]\oint \mathrm{d}s_k.\end{aligned}$$

Assuming that $\phi(\mathbf{x},t,\mathbf{\Omega},E)$ is spatially smooth, the integral of $\tilde{F}_{g,m,k}$ with $\mathbf{\Omega}$ is,

$$\begin{aligned}\tilde{\mathcal{F}}_{g,k}=&v_g\sum_{g'}\varphi^{p+1}_{g',k}\sum_m\omega_m\dot{\Omega}_{m,k}\varsigma^*_{g'\to g,m,i}\oint \mathrm{d}s_k\\&-\tau_g v_g^2\sum_{g'}\Big(\nabla\varphi^{p+1}_{g',k}\cdot\mathbf{n}_k\Big)\sum_m\omega_m\dot{\Omega}^2_{m,k}\varsigma^*_{g'\to g,m,i}\oint \mathrm{d}s_k.\end{aligned}$$

According to Eq. (4.3) and the detailed analysis of scattering coefficients in Appendix C, the first term in $\tilde{\mathcal{F}}_{g,k}$ can be rearranged as,

$$\begin{aligned}&v_g\sum_{g'}\varphi^{p+1}_{g',k}\sum_m\omega_m\dot{\Omega}_{m,k}\varsigma^*_{g'\to g,m,i}\\=&\sum_{g'}\sigma_{1,g'\to g}\varphi^{p+1}_{g',k}(<\Omega_1 h^p_{g'}>,<\Omega_2 h^p_{g'}>,<\Omega_3 h^p_{g'}>)\cdot(n_{k,1},n_{k,2},n_{k,3})^T\\=&v_g\mathbf{J}^{p+1}_{g,k}\cdot\mathbf{H}_{g'}\cdot\mathbf{n}_k\sum_{g'}\sigma_{1,g'\to g}.\end{aligned}$$

Here the matrix related with $<\Omega_i h_{g'}>$ is defined as,

$$\mathbf{H}_{g'}=\begin{pmatrix} \frac{<\Omega_1 h^p_{g'}>}{<\Omega_1 h^{p+1}_{g'}>} & 0 & 0 \\ 0 & \frac{<\Omega_2 h^p_{g'}>}{<\Omega_2 h^{p+1}_{g'}>} & 0 \\ 0 & 0 & \frac{<\Omega_3 h^p_{g'}>}{<\Omega_3 h^{p+1}_{g'}>} \end{pmatrix}. \tag{4.11}$$

The second term of $\mathcal{F}^{p+1}_{g,k}$ is rewritten as,

$$\begin{aligned}&\tau_g v_g^2 \sum_{g'}\left(\nabla\varphi^{p+1}_{g',k}\cdot\mathbf{n}_k\right)\sum_m \omega_m \dot{\Omega}^2_{m,k}\varsigma^*_{g'\to g,m,i}\\ =&\tau_g v_g^2 \sum_{g'}\mathbf{n}_k\cdot\left(\sum_m \omega_m \mathbf{\Omega}_m\mathbf{\Omega}_m\varsigma^*_{g'\to g,m,i}\right)\cdot\nabla\varphi^{p+1}_{g',k}.\end{aligned}$$

Define $3\sum_m \omega_m \mathbf{\Omega}_m\mathbf{\Omega}_m\varsigma^*_{g'\to g,m,i}$ as the effective secondary neutron number $\mathbf{C}_{eff,g}$, which has the following forms,

$$\begin{aligned}\mathbf{C}_{eff,g}=&\sum_{g'}(\sigma_{0,g'\to g}-\sigma_{2,g'\to g})\mathbf{I}\\ &+3\sum_{g'}\sigma_{2,g'\to g}\begin{pmatrix} <\Omega_1\Omega_1 h^p_{g'}> & <\Omega_1\Omega_2 h^p_{g'}> & <\Omega_1\Omega_3 h^p_{g'}> \\ <\Omega_1\Omega_2 h^p_{g'}> & <\Omega_2\Omega_2 h^p_{g'}> & <\Omega_2\Omega_3 h^p_{g'}> \\ <\Omega_1\Omega_3 h^p_{g'}> & <\Omega_2\Omega_3 h^p_{g'}> & <\Omega_3\Omega_3 h^p_{g'}> \end{pmatrix}.\end{aligned}$$

Therefore, it can be derived that the diffusion coefficients is tensor form in the anisotropic scattering model,

$$\mathbf{D}_g=\frac{1}{3}\left(\mathbf{I}-\chi\mathbf{H}_g\right)^{-1}\cdot\mathbf{C}_{eff,g},$$

where

$$\chi_g=\sum_{g'}\sigma_{1,g'\to g}.$$

According to the definition of $\mathbf{D}_g$, it is easily get that in the case of strong anisotropy, the explicit prediction of h_g by using p-th step has influences on the equivalent diffusion coefficient. This may affect the convergence rate of the numerical scheme. When the iteration get converged with $h^p=h^{p+1}$ and the distribution of ϕ is approximately isotropic, the diffusion coefficient can reduce to scalar,

$$D_g=\frac{C_{eff,g}}{3\Sigma_g\left(1-\chi_g\right)},\quad C_{eff,g}=\sum_{g'}(\sigma_{0,g'\to g}+\sigma_{2,g'\to g}).$$

The numerical flux $\tilde{\mathcal{F}}_{g,k}$ can be simplified as,

$$\tilde{\mathcal{F}}_{g,k}^{p+1}=-v_g\left[D_{g,k}\nabla\varphi_{g,k}^{p+1}\cdot\mathbf{n}_k\right]_{s_l}\oint \mathrm{d}s_k.$$

Thus the discrete equation of φ_g is (considering $\epsilon=0$ to simplify the derivation),

$$\frac{\varphi_{g,i}^{p+1}-\varphi_{g,i}^{n}}{v_g\Delta t_P}-\frac{1}{V_i}\sum_l\left(D_{g,k}\nabla\varphi_{g,k}^{p+1}\cdot\mathbf{n}_k\oint \mathrm{d}s_k\right)+\Sigma_{g,i}\varphi_{g,i}^{p+1}=\sum_{l=0}^{L}\sum_{g'}\varphi_{g',i}^{p+1}\sum_m\varsigma_{g'\to g,m,i}^{p+1}. \tag{4.12}$$

Eq. (4.12) is exactly the discrete form of the diffusion equation,

$$\begin{aligned}&\frac{1}{v(E)}\frac{\partial\varphi(\mathbf{x},t,E)}{\partial t}-\nabla\cdot(D(\mathbf{x},E)\nabla\varphi(\mathbf{x},t,E))+\Sigma(\mathbf{x},E)\varphi(\mathbf{x},t,E)\\&=\int \mathrm{d}\mathbf{\Omega}\int \mathrm{d}\mathbf{\Omega}'\int \mathrm{d}E'\Sigma(\mathbf{x},E')f(\mathbf{x},\mathbf{\Omega}',E'\to\mathbf{\Omega},E)\phi(\mathbf{x},t,\mathbf{\Omega}',E').\end{aligned}$$

At this point, we have completed the analysis of the AP property of IUGKS-AM.

In some special cases, the diffusion coefficient $D_{g,k}$ can be given in the usual form. For the P1 case as example, it has,

$$D_g=\frac{C_{eff,g}^0}{3\Sigma_g\left(1-\chi_g\right)},\quad C_{eff,g}^0=\sum_{g'}\sigma_{0,g'\to g}.$$

For isotropic multi-group case, it has,

$$D_g=\frac{C_{eff,g}^0}{3\Sigma_g}.$$

For monoenergetic case, it has

$$D=\frac{1}{3\Sigma}.$$

The forms of D_g or D are exactly the diffusion coefficients under corresponding conditions.

5 Numerical tests

In this section, the developed IUGKS-AM is tested comprehensively by several numerical examples.

5.1 Scheme accuracy test

The transport equation of 1D case can be simplified as,

$$\frac{\partial\phi(x,\mu,t)}{\partial t}+\mu\frac{\partial}{\partial x}\phi(x,\mu,t)+\Sigma\phi(x,\mu,t)=\frac{1}{2}\int\Sigma_s\phi(x,\mu',t)\mathrm{d}\mu'+q(x,\mu,t).$$

The exact solution of ϕ is,

$$\phi(x,\mu,t)=(\mu+1)\cos^2\pi(x+t).$$

The computation domain is $[0,1]$, and the grids $N=10,20,40,80$ and 160 are used to verify the scheme accuracy in unsteady simulations. The time step is set as $2.5/N$, which varies in proportion to the grid size The simulation time is set as $t=2$ which is two time cycles. The discrete ordinate number is $M=2$. The cross-section parameter is Σ, and we considered two models with different scattering coefficients,

$$\begin{cases}\Sigma_s=\Sigma, & \text{isotropic P0 case;}\\ \Sigma_s=\Sigma(1+\mu\mu'), & \text{anisotropic P1 case.}\end{cases}$$

The external source terms for the two cases are respectively,

$$\begin{cases}q=-(\mu+1)^2\pi\sin2\pi(x+t)+\Sigma\mu\cos^2\pi(x+t), & \text{P0 case;}\\ q=-(\mu+1)^2\pi\sin2\pi(x+t)+\frac{2\Sigma\mu}{3}\cos^2\pi(x+t), & \text{P1 case.}\end{cases}$$

Table 1 is the scheme accuracy of IUGKS-AM in the anisotropic P1 scattering model. The results firstly shows that, IUGKS-AM can achieve the designed 2nd-order under both transport and diffusion conditions. In addition, the case also indicates that omitting the time derivative term of $S_g(\mathbf{x},t)$ in the flux of IUGKS-AM has few effects on the scheme time accuracy. This validates the rationality of the flux simplification in Eq. (3.8).

According to the construction of IUGKS-AM, the scheme should return to IUGKS scheme in isotropic models. We further simulate the P0 model to verify the scheme performances in the simplified models, which is shown in Table 2. Furthermore, by comparing Tables 1 and 2, it can be seen that the absolute errors of IUGKS-AM in P1 model keep consistent with that in P0 model. This conclusion verifies that the assumptions introduced in Eq. (4.4) have limited effects on the convergence accuracy of the scheme.

Table 1: The scheme accuracy of IUGKS-AM for P1 model.

	$\Sigma=2$			$\Sigma=2000$		
N	$\lg L_\infty$	$\lg L_2$	Order	$\lg L_\infty$	$\lg L_2$	Order
10	-1.19	-0.92	–	-1.52	-1.25	–
20	-1.79	-1.61	2.01	-2.60	-2.21	3.60
40	-2.39	-2.16	1.99	-3.44	-2.88	2.78
80	-2.99	-2.79	2.01	-4.19	-3.52	2.49
160	-3.60	-3.38	2.01	-4.87	-4.20	2.29

Table 2: The scheme accuracy test for P0 model.

	$\Sigma=2$			$\Sigma=2000$		
N	$\lg L_\infty$	$\lg L_2$	Order	$\lg L_\infty$	$\lg L_2$	Order
10	-1.16	-0.90	–	-1.53	-1.26	–
20	-1.76	-1.57	2.01	-2.61	-2.22	3.60
40	-2.36	-2.12	1.99	-3.45	-2.90	2.79
80	-2.96	-2.74	2.01	-4.20	-3.54	2.51
160	-3.56	-3.34	2.01	-4.92	-4.23	2.40

5.2 1D unsteady monoenergetic case

In 1D monoenergetic case, the neutron equation is quite simple, so that IUGKS-PN scheme is relatively easy to implement. Therefore, IUGKS-PN is used as reference to quantitatively analyze the performances of IUGKS-AM under different computation conditions in this case. In addition, we also implement FV-SI algorithm for comparison. In FV-SI, the differential and integral terms of the transport equation are solved by splitting method, and the source iteration (SI) is employed to update the equation. The spatial discretization method is FV scheme, while the upwind numerical flux is,

$$F_{g,m,k}=\dot{\xi}_{g,m,k}\left(\phi^L_{g,m,k}\mathrm{H}[\dot{\Omega}_{m,k}]+\phi^R_{g,m,k}\mathrm{H}[-\dot{\Omega}_{m,k}]\right).$$

The fully discrete form of the time implicit scheme has the same form as Eq. (3.14).

The computational domain is $[0,2]$, while the grid size is N=200. The discrete ordinate number is $M=100$. The initial distribution of the neutron flux ϕ is,

$$\phi(x,0,\mu)=\begin{cases}2, & 0.8<x<1.2,\\ 0, & \text{otherwise.}\end{cases}$$

The maximum permission error of converge criterion for the inner iteration is 10^{-3}. The scattering coefficient is,

$$\Sigma(\mathbf{x})f(\mathbf{x},\mathbf{\Omega}'\to\mathbf{\Omega})=\Sigma(x)(1+f_1\mu\mu').$$

We consider two cases with different forms of $\Sigma(\mathbf{x})$ and $f(\mathbf{x},\mathbf{\Omega}'\to\mathbf{\Omega})$, while the form of $f(\mathbf{x},\mathbf{\Omega}'\to\mathbf{\Omega})$ are the isotropic P0 condition $f_1=0$ and the anisotropic P1 condition $f_1=1$.

5.2.1 Case 1

The cross section $\Sigma(x)$ is,

$$\Sigma(x)=\begin{cases}0.02\sigma, & x\in[0.35,0.65]\cup[1.35,1.65],\\ \sigma, & x\in[0,0.35)\cup(0.65,1.35)\cup(1.65,1].\end{cases}$$

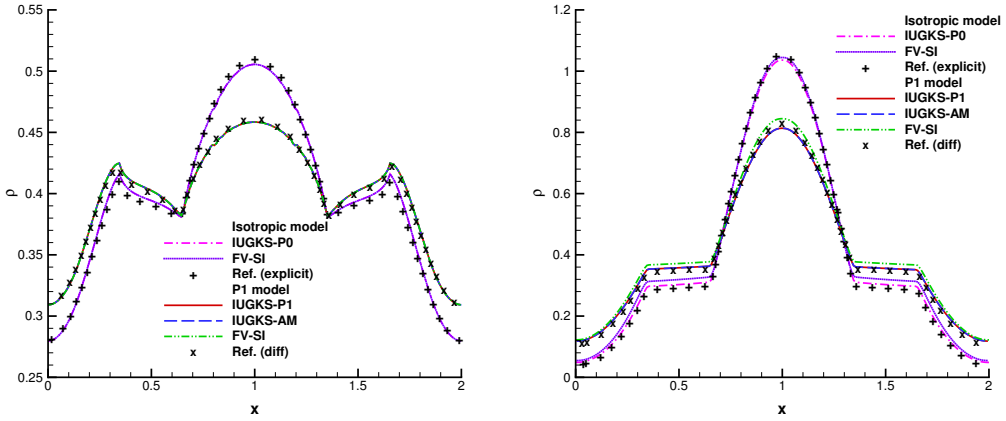

Figure 1: Distributions of ρ for Case 1: $\sigma=1$ (left) and 10^3 (right).

σ is set as 1 and 10^3, while the computation time $t_{\max}$ is set as 1 and 0.1, respectively. The time step Δt_p is set as $\Delta x/3$.

Fig. 1 shows the computational results of ρ,

$$\rho=\frac{1}{2}\int_{-1}^{1}\phi(x,t,\mu)\mathrm{d}\mu.$$

The Ref. data are solutions calculated by the explicit solver and the diffusion solver of Li [24]. In the four cases of computation conditions, the results of IUGKS-PN, IUGKS-AM are consistent with Ref., which firstly verifies the correctness of the numerical schemes in different conditions.

5.2.2 Case2

The cross section $\Sigma(x)$ is,

$$\Sigma_0(x)=100(x-1)^4\sigma.$$

σ is set to 1 and 10^3, while the computation physical time $t_{\max}$ is set as 1 and 0.1, respectively. The physical time step Δt_p is $\Delta x/15$.

Fig. 2 shows the computational results of ρ, in which the results of IUGKS-PN and IUGKS-AM are all in agreements with the reference data.

In these two cases, the computational grid Kn number varies greatly with different σ values. Especially for Case 2, when $\sigma=1000$, the grid Kn number is $[0,10^3]$ within the computation domain, which covers the free transport to diffusion limit condition. Thus the case is very challenging.

In Figs. 1 and 2, when $\sigma=1$, the calculation results of different numerical schemes are basically the same. When $\sigma=1000$, the computational results obtained by the UGKS methods exhibit significant differences from those obtained from the SI method. Along

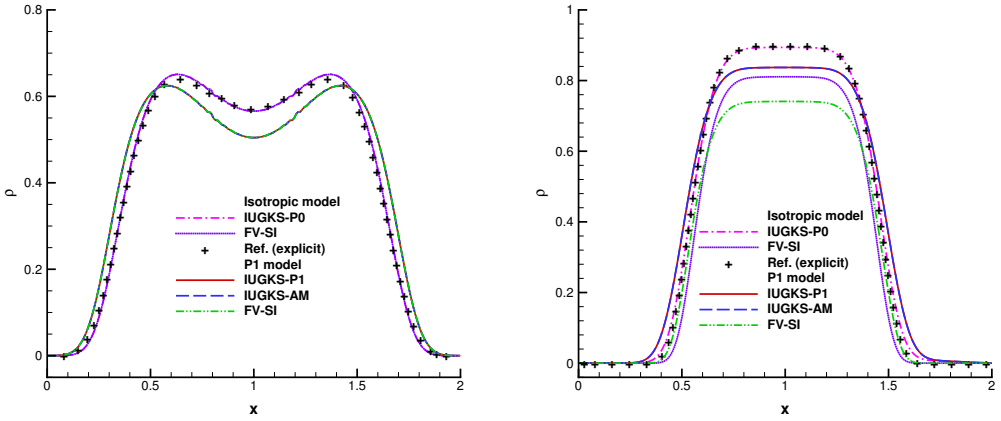

Figure 2: Distributions of ρ for case 2: $\sigma=1$ (left) and 10^3 (right).

Table 3: Average iteration number per time step of different schemes.

Scattering model	Numerical scheme	Case 1		Case 2	
		$\sigma=1$	$\sigma=10^3$	$\sigma=1$	$\sigma=10^3$
Isotropic	IUGKS-P0	3.6	73.3	3.0	34.0
	FV-SI	3.6	6106.6	3.0	1437.3
P1	IUGKS-P1	3.6	69.3	3.0	34.0
	IUGKS-AM	3.6	69.3	3.0	34.0
	FV-SI	3.6	6375.4	3.0	1534.3

with the data in Table 3, our analysis of the numerical schemes is as follows. Firstly, under the condition of free transport limit, all numerical schemes can maintain ideal convergence accuracy and speed. Secondly, under the diffusion limit with a large grid Kn number, the performances of different numerical schemes vary greatly. Among them, IUGKS-AM is consistent with the reference solution of IUGKS-PN and the diffusion scheme. The calculation of FV-SI is affected by the stiffness of the collision term, resulting in significant numerical dissipation and differences in the calculation results. Finally, comparing the number of iterations in Table 3, it can be seen that the convergence speed of FV-SI decreases at the diffusion limit. Therefore, through this example, we have verified that the AP property of multi-scale methods enables the scheme to maintain ideal convergence speed and accuracy under a wide range of computational conditions for both isotropic and anisotropic models. Furthermore, the IUGKS-AM developed in this paper exhibits similar numerical performances with the IUGKS-PN method in above cases.

In case 2, we further test IUGKS-AM in different degrees of anisotropy models. The calculation results are shown in Table 4. The time $t_{\max}$ is set as 0.5. When $\Sigma=1$, as the anisotropy of the model increases (that f_1 becomes larger), the average iteration number

Table 4: Average iteration number of different scattering coefficient.

		$f_1=1$	$f_1=2$	$f_1=3$
IUGKS-P1	$\Sigma=1$	3.0	3.0	3.0
IUGKS-AM		3.0	3.0	3.0
IUGKS-P1	$\Sigma=10$	3.4	3.4	3.7
IUGKS-AM		3.5	4.1	10.9

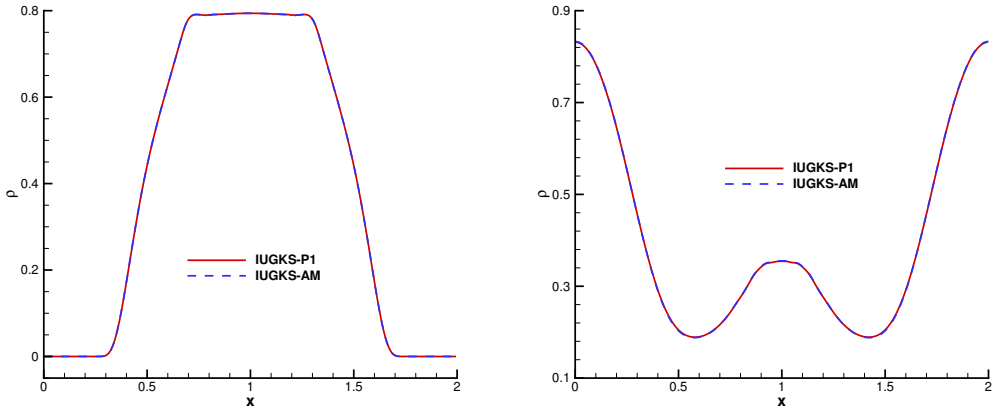

Figure 3: Distributions of ρ for case 2 with $f=3$: $\sigma=1$ (left) and 10 (right).

of IUGKS-AM is basically the same as that of IUGKS-P1. With $\Sigma=10$, the iteration steps required for IUGKS-AM increase compared with IUGKS-P1 when f_1 is large, while the result of IUGKS-AM is still consistent with IUGKS-P1 shown in Fig. 3.

In this case, we verify that IUGKS-AM keeps good numerical properties in large-range conditions when the model anisotropy is low. In strong anisotropy models, IUGKS-AM can still obtain numerical results agree with IUGKS-PN, but it needs more iterative steps. The numerical tests are consistent with the analysis in Section 4.2.

5.3 2D anisotropic scattering case

The geometry and boundary conditions are shown in Fig. 4. The south boundary is inflow with $\phi_w=1$, and the other boundaries are set vacuum. The computational domain is $[0,1]\times[0,1]$, and the grid size is $N=26\times26$. The discrete ordinate is S_{16} without remarks.

The scattering coefficient is,

$$\Sigma(\mathbf{x})f(\mathbf{x},\boldsymbol{\Omega}'\to\boldsymbol{\Omega})=\Sigma\sum_{l=0}^{L}\frac{2l+1}{4\pi}f_lP_l(\boldsymbol{\Omega}'\cdot\boldsymbol{\Omega}),$$

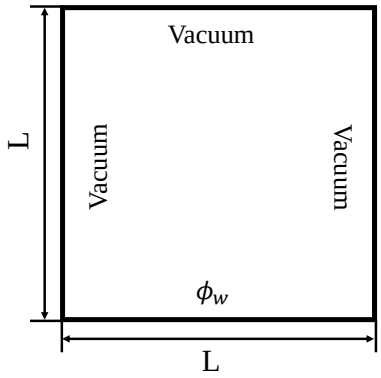

Figure 4: Geometry and boundary conditions.

Table 5: Coefficients f_l for different cases.

l	Iso	F_1	F_2	B_1	B_2
0	1.00000	1.00000	1.00000	1.00000	1.00000
1		2.53602	2.00917	-0.56524	-1.20000
2		3.56549	1.56339	0.29783	0.50000
3		3.97976	0.67407	0.08571	
4		4.00292	0.22215	0.01003	
5		3.66401	0.04725	0.00063	
6		3.01601	0.00671		
7		2.23304	0.00068		
8		1.30251	0.00005		
9		0.53463			
10		0.20136			
11		0.05480			
12		0.01099			

where Σ is the total cross section, and $P_l(\mathbf{\Omega}'\cdot\mathbf{\Omega})$ is the l-th Legendre polynomials in 1D case. Five cases with different order of $f(\mathbf{x},\mathbf{\Omega}'\to\mathbf{\Omega})$ are calculated, and the coefficients f_l are given in Table 5. And in the following text, we use symbols in Table 5 to mark cases with different calculation conditions. The physical quantities φ, Q_x and Q_y for this case are defined as,

$$\varphi(\mathbf{x}) = \int \phi(\mathbf{x},\mathbf{\Omega})\mathrm{d}\mathbf{\Omega},$$
$$Q_x(\mathbf{x}) = \int \Omega_x\phi(\mathbf{x},\mathbf{\Omega})\mathrm{d}\mathbf{\Omega},$$
$$Q_y(\mathbf{x}) = \int \Omega_y\phi(\mathbf{x},\mathbf{\Omega})\mathrm{d}\mathbf{\Omega}.$$

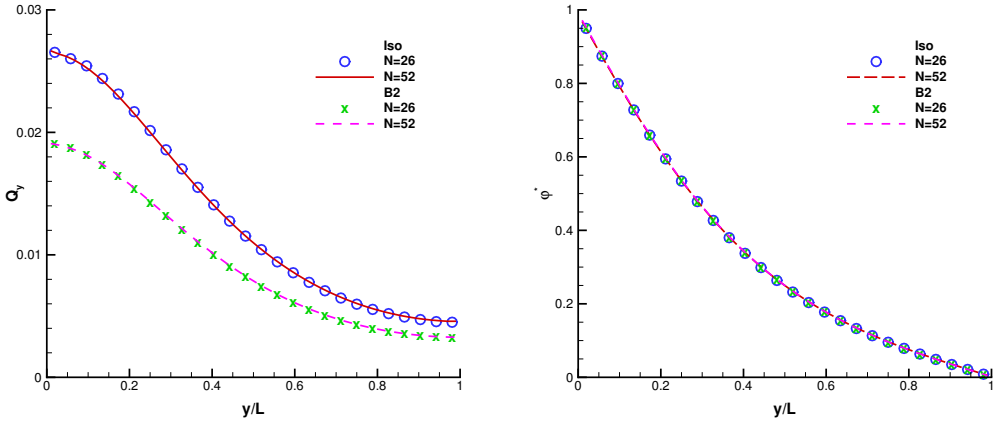

Figure 5: Q_y and φ at $x=0.5$ for Iso and B_2 with $\sigma=100$ in different grids.

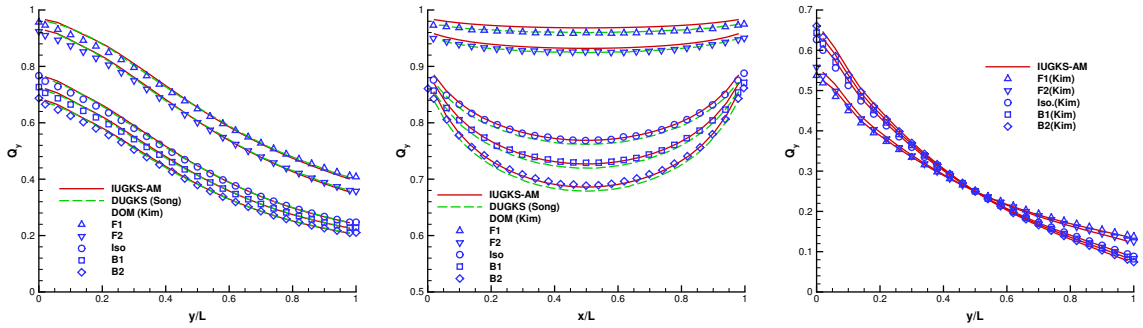

Figure 6: Q_y at $x=0.5$ (left), Q_x at $y=0$ (middle) and $\varphi(\mathbf{x})$ at $x=0.5$ (right) of different models.

Firstly, we use the Iso and B_2 cases to verify the grid convergence. For transport equation calculations, the challenges for numerical calculation are greater with larger grid Kn number. So we use the condition $\Sigma=100$ to verify the convergence of spatial grid scale. The computational grids are 26×26 and 52×52, respectively. The used discrete ordinate is S_8. The computational results in Fig. 5 show that the computation results of refined grid are consistent with those of coarse grid. Therefore, it can be considered that the calculation by using a 26×26 grid has reached grid convergence and will be used in the following tests.

In Fig. 6, from left to right, the results are Q_y at $x=0.5$, Q_x at $y=0$ and φ at $x=0.5$ with $\Sigma=1$. IUGKS-AM gets good agreements with the reference results of DOM [25] and DUGKS [22] in different scattering models. The simulations verify the accuracy of IUGKS-AM in two-dimensional anisotropic scattering models, which also show that the scheme has good accuracy in complex scattering models.

We further calculate the F2 model with $\Sigma\in[0.01,100]$ to test the scheme performances

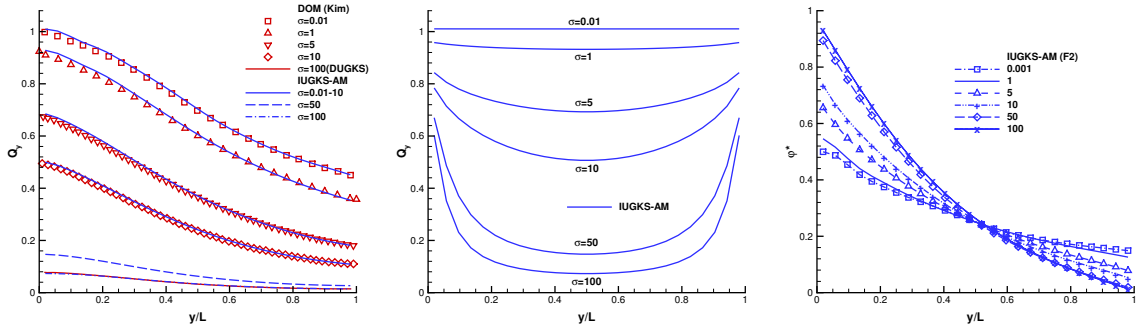

Figure 7: Q_y at $x=0.5$ (left), Q_x at $y=0$ (middle) and $\varphi(\mathbf{x})$ at $x=0.5$ (right) for F2 model with different Σ.

in large-range conditions. Fig. 7 shows that IUGKS-AM is in good agreements with the reference DOM results for all Σ cases. With the increase of Σ, the free transport effect weakens and the particle diffusion is confined within a small region near the incident boundary. When $\Sigma \geq 5$, DOM requires a refined grid as 52×52. However, IUGKS-AM, which has good AP properties in diffusion limit, can still get ideal calculation results with coarser 26×26 grid even with larger Σ conditions.

The geometry and boundary conditions of this case are simple, whereas the anisotropic-scattering models are quite complex. In this case, IUGKS-AM shows good numerical properties in high-order scattering models with a large range of computational conditions.

5.4 1D multi-group anisotropic scattering cases

In this case, two multi-group anisotropic-scattering models are simulated by IUGKS-AM.

5.4.1 Case 1: 2-group P3 model

The first case is a simplified model with two regions and two energy group. The scattering coefficients is approximated by P3 Legendre expansion. The geometry and boundary conditions are shown in Fig. 8.

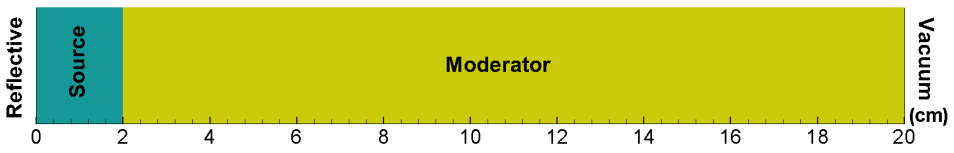

Figure 8: Geometry for two-region P_3 scattering case.

Table 6: Cross sections and external source for different regions.

	Group 1		Group 2	
	Source	Moderator	Source	Moderator
q	1	0	1	0
Σ	1	1	1	0
$\Sigma_{s,0}(g\to g)$	1/2	1/2	1/2	1/2
$\Sigma_{s,0}(g-1\to g)$	-	-	1/2	1/2
$\Sigma_{s,1}(g\to g)$	9/10	9/10	9/10	9/10
$\Sigma_{s,1}(g-1\to g)$	-	-	9/10	9/10
$\Sigma_{s,2}(g\to g)$	1	1	1	1
$\Sigma_{s,2}(g-1\to g)$	-	-	1/5	1
$\Sigma_{s,3}(g\to g)$	3/5	3/5	3/5	3/5
$\Sigma_{s,3}(g-1\to g)$	-	-	3/5	3/5

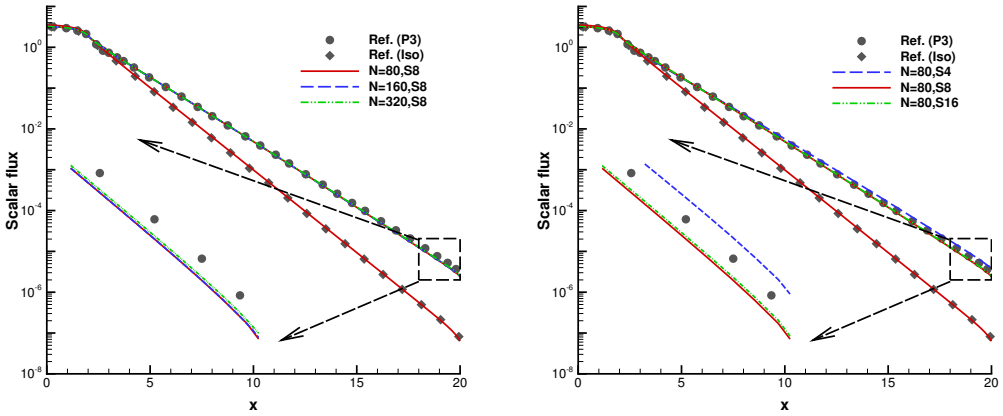

Figure 9: Group 2 scalar flux with different grids and S_n settings calculated by IUGKS-AM.

The 2-group P3 scattering coefficient for 1D geometry is,

$$\Sigma(\mathbf{x},E')f(E'\to E,\boldsymbol{\Omega}\cdot\boldsymbol{\Omega}')=\sum_{l=0}^{3}\frac{2l+1}{4\pi}\Sigma_{s,l}(E'\to E)P_l(\boldsymbol{\Omega}'\cdot\boldsymbol{\Omega}). \tag{5.1}$$

The cross section Σ, coefficients $\Sigma_{s,l}(E'\to E)$ and the external source terms for different group in source and moderator regions are given in Table 6.

By using different grid sizes and discrete ordinate, the calculation convergence is checked. The computational results of $\varphi=\int\phi(x,\Omega)\mathrm{d}\Omega$ are shown in Fig. 9. The simulation results with the grid with $N=80$ and S_8 can be considered as the convergent solution, and the simulation results agree well with the reference data of [26]. The same results is hold for the isotropic simulation.

5.4.2 Case 2: 3-group P1 model

The second case is a 1D section of the 2D axisymmetric KAPL (Knolls Atomic Power Laboratory) with dog-leg void model [26–28]. The geometry and boundary conditions are shown in Fig. 10, which contains seven material regions. Three neutron groups are simulated. In the source region (I), the external source term for each group is,

$$q_1 = 0.097702, \quad q_2 = 0.45451, \quad q_3 = 0.44610.$$

The 3-group P1 scattering term is,

$$\Sigma(\mathbf{x},E')f(E'\to E,\boldsymbol{\Omega}\cdot\boldsymbol{\Omega}') = \sum_{l=0}^{1}\frac{2l+1}{4\pi}\Sigma_{s,l}(E'\to E)P_l(\boldsymbol{\Omega}'\cdot\boldsymbol{\Omega}).$$

The values of $\Sigma(E)$ and $\Sigma_{s,l}(E'\to E)$ are given in Appendix D.

Firstly, we use the isotropic scattering condition to verify the grid convergence of this model. According to the computational results in Fig. 11, the computational results with $N=65$ and S_8 can be considered as the converged results. This calculation condition is adopted in the following numerical calculation and analysis without remarks.

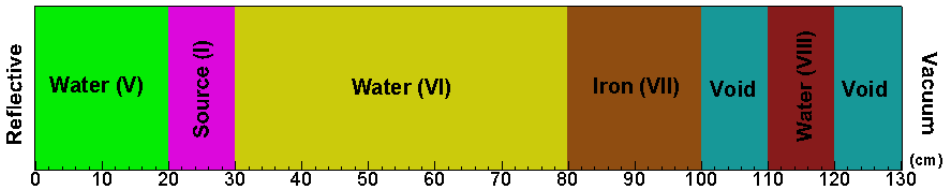

Figure 10: Geometry for seven-region P_1 scattering case.

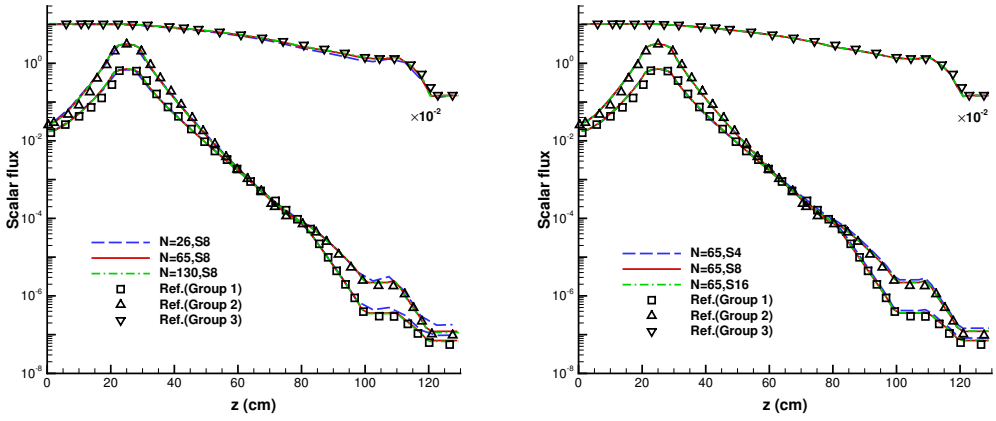

Figure 11: Grid convergence test with isotropic scattering. The scalar flux of group 3 in the figure is 10^{-2} times the original value.

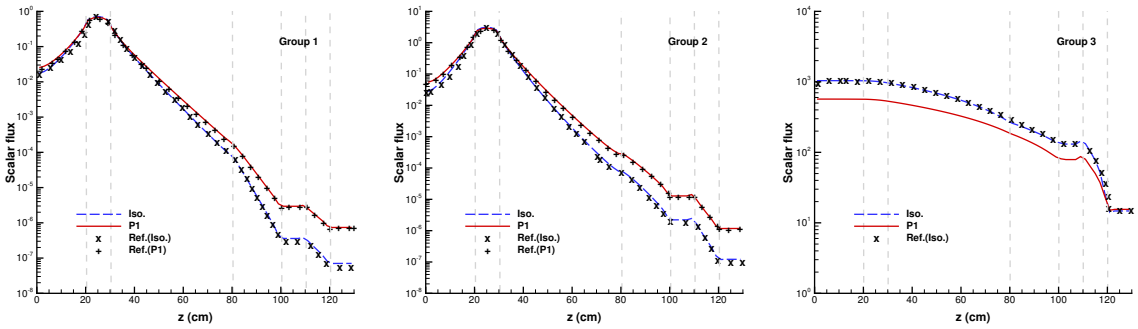

Figure 12: Simulation results of isotropic and P1 anisotropic scattering for different group with IUGKS-AM.

Table 7: Averaged scalar flux for isotropic and P_1 anisotropic scattering.

	Isotropic			Anisotropic		
Region	Group 1	Group 2	Group 3	Group 1	Group 2	Group 3
1	9.2022E-2	3.0122E-1	1.0393E3	9.9224E-2	3.4399E-1	5.6868E2
2	6.4616E-1	2.8278E0	1.0128E3	6.1755E-1	2.6597E0	5.5452E2
3	3.6945E-2	1.2064E-1	6.1828E2	3.9897E-2	1.3787E-1	3.6066E2
4	1.5857E-5	2.7171E-5	1.9800E2	4.6106E-5	1.0933E-4	1.3234E2
5	3.6406E-7	2.2615E-6	1.3431E2	2.9855E-6	1.3102E-5	8.0935E1
6	1.8224E-7	7.0752E-7	7.8052E1	1.5982E-6	4.6453E-6	5.0740E1
7	7.0480E-8	1.2142E-7	1.4603E1	7.3869E-7	1.1725E-6	1.5437E1

Fig. 12 shows the simulation results for isotropic and P1 anisotropic scattering coefficients, which are further compared with the reference data from [27,29]. The calculations IUGKS-AM agree well with the reference solutions of three neutron groups for both conditions. Compared with isotropic model, the anisotropic effect weakens the scattering of high-energy neutrons to thermal groups.

Table 7 gives the average scalar flux for each region in detail. The difference between isotropic scattering and anisotropic scattering can be quantitatively compared. Under the condition of anisotropic scattering, the number of neutrons in the first six regions is reduced by $35-45\%$ for the thermal group.

In these two cases, IUGKS-AM show good agreements with the reference results in all kinds of models. The correctness and reliability of the scheme in complex model with multi-group and anisotropic scattering conditions are verified.

5.5 3D multi-group KAPL model

Through the above scheme validation in various scattering models and multi-group conditions, we further simulate the 3D model with complex geometric conditions in this case.

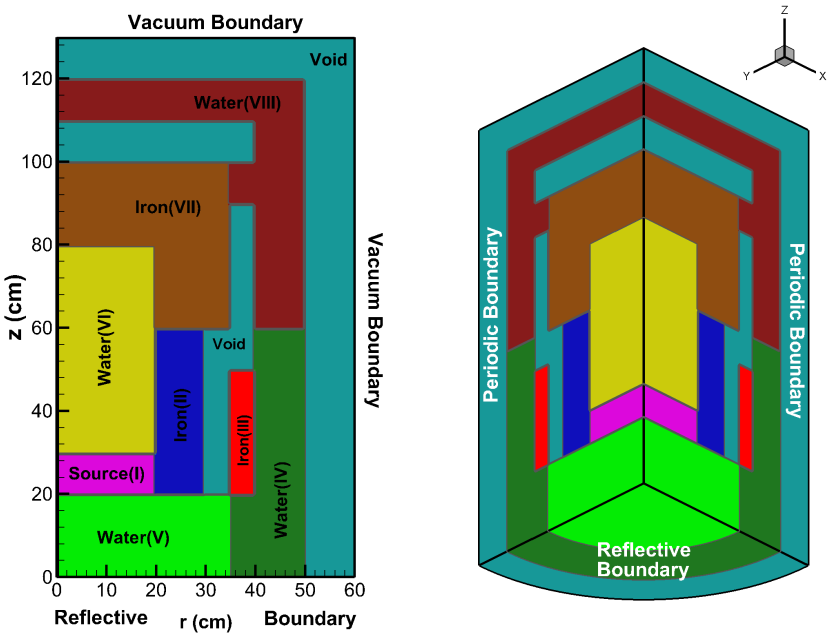

Figure 13: Geometry and parameter distributions for 3D cylinder case.

As shown in Fig. 13, the material distribution of 3D KAPL model is complex, and its geometry is rotationally symmetric. In Asaoka's work [28], the 2D (r,z) axisymmetric method is used to calculate the model. In this paper, we calculate this case directly in 3D (x,y,z) Cartesian coordinates. The $1/4$ model is simulated and the boundaries of $\theta=0$ and $\theta=\pi/2$ are set to be periodic as Fig. 13. The 3-group external source term and collision term are same as case 5.4.2, while the model coefficients of each region are shown in Appendix D.

According to the convergence verification results of case 5.4.2, S_8 is adopted in the $\mathbf{\Omega}$ direction, while the grid $30\times65\times6$ (G1) can be used in $r-z$ plane. However, considering the more complex geometric structure of the 3D model, the encrypted grid $60\times130\times12$ (G2) is further used to confirm the grid convergence. In addition, the θ-direction grid scale is also verified in G1 and G2 with grid number 6 and 12, respectively.

Figs. 14 and 15 show the results of the neutron scalar flux at $r=356.25$cm and $z=103.75$cm, respectively. Firstly, by comparing the results of G1 and G2, it can be get that the calculations of IUGKS-AM have basically reached the grid convergence. In the region far away from the external source, due to that the neutron flux is relatively small, higher grid resolution is needed to accurately capture neutron distribution. The simulation results are basically consistent with the reference data [28], while IUGKS-AM shows better grid convergence.

Fig. 16 shows the contours of neutron scalar flux with isotropic and anisotropic P1 scattering models. The anisotropic influences are not obvious in source region for group-

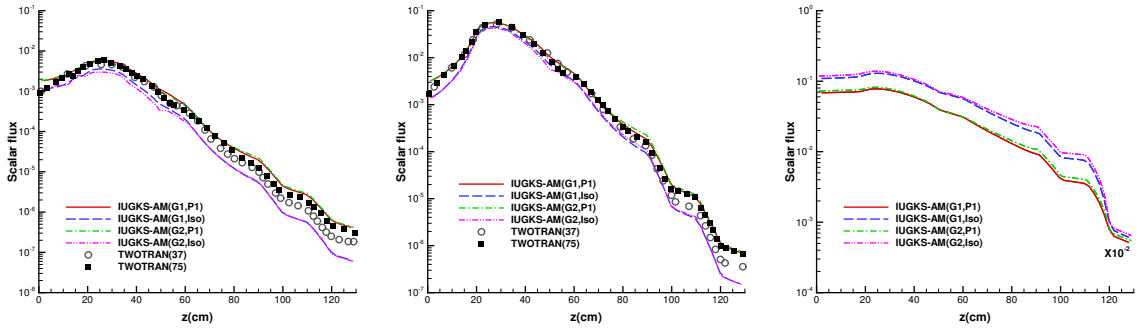

Figure 14: Scalar flux on line $r=36.25$ cm.. TWOTRAN(37): 1248 cells in $r-z$ plane and S_6; TWOTRAN(75): 4992 cells in $r-z$ plane and S_{16} [28].

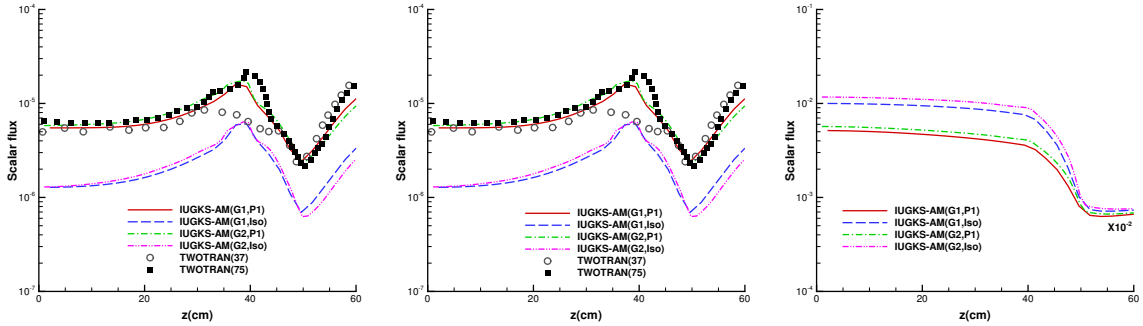

Figure 15: Scalar flux on line $z=103.75$ cm. TWOTRAN(37): 1248 cells in $r-z$ plane and S_6; TWOTRAN(75): 4992 cells in $r-z$ plane and S_{16} [28].

1 and group-2, where the neutron distributions are mainly determined by the external source term. In regions far from the source region, differences of neutron scalar fluxes are distinct. For the thermal group, the influences of anisotropic scattering coefficients are notable in the whole computation domain.

In this case, we use IUGKS-AM to simulate the 3D anisotropic scattering model with multi-group parameters. The model and computation conditions are relatively complex, which is closer to the real engineering application. Based on this numerical test, IUGKS-AM shows a good application prospect in practical engineering complex problems.

6 Conclusion

In order to meet the requirements of neutron transport simulation in complex engineering applications, this paper develops IUGKS-AM based on the isotropic scattering IUGKS framework, which is applicable to arbitrary anisotropic scattering model. In IUGKS-AM, the high-order moments of neutron flux are estimated by the low-order moment.

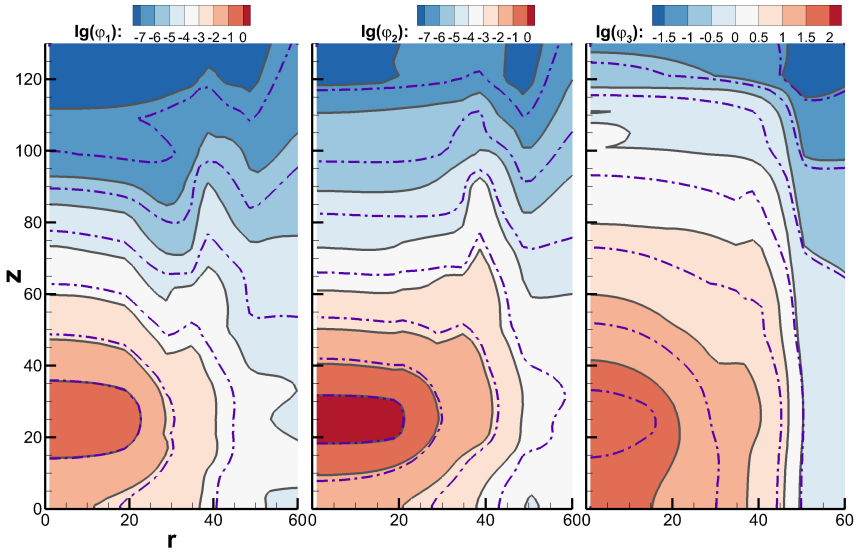

Figure 16: Contours of neutron scalar flux with different scattering coefficients (isotropic case: colored regions and solid gray lines; anisotropic case: dash-dot purple lines).

The scheme discretization does not introduce macro auxiliary solutions of higher-order moment equations. Therefore, IUGKS-AM has stronger universality and extensibility, which is also easier to implement in code. A detailed analysis of the AP properties of IUGKS-AM at the diffusion limit is provided in the paper. In addition, the differences between the scheme and IUGKS-PN were qualitatively/quantitatively compared numerically through typical cases. The IUGKS-PN scheme rigorously calculates the high-order moment auxiliary equations corresponding to each anisotropic scattering PN expansion term. Through the analysis and numerical testing, it has been proven that IUGKS-AM maintains good convergence and computational accuracy under a wide range of grid Kn numbers. In the numerical tests, the correctness and reliability of IUGKS-AM in the calculations of complex neutron transport model equations are comprehensively verified from the perspectives of different group parameters and different order anisotropic scattering models through typical 1D/2D/3D cases. The work promotes the application and development of IUGKS in practical transport simulations, and provides a novel numerical method for the calculation of complex 3D neutron anisotropic scattering transport equations.

Acknowledgments

The current research is supported by NSFC (Grant No. 12572329, Grant No. 12372285) and by Beijing Natural Science Foundation(Grant No. Z230003).

Appendices

A Anisotropic collision term

In this appendix, the specific form of collision term of three-dimensional anisotropic scattering model is given.

In 3D case, the expansion of $f(E\to E',\mathbf{\Omega}\cdot\mathbf{\Omega}')$ in Eq. (2.2) is,

$$f(\mathbf{x},\mathbf{\Omega}',E'\to\mathbf{\Omega},E)=\sum_{l=0}^{L}\sum_{r=-l}^{l}f_l(\mathbf{x},E'\to E)Y_{lr}(\theta,\omega)Y_{lr}^*(\theta',\omega'). \tag{A.1}$$

Here $Y_{lr}(\theta,\omega)$ is spherical harmonic function, while $Y_{lr}^*(\theta,\omega)$ denotes the complex conjugate of $Y_{lr}(\theta,\omega)$,

$$Y_{lr}(\theta,\omega)=\left[\frac{(2l+1)(l-r)!}{4\pi(l+r)!}\right]^{1/2}P_l^r(\cos\theta)\mathrm{e}^{ir\omega},$$
$$Y_{lr}^*(\theta,\omega)=\left[\frac{(2l+1)(l-r)!}{4\pi(l+r)!}\right]^{1/2}P_l^r(\cos\theta)\mathrm{e}^{-ir\omega}.$$

Y_{lr} and Y_{lr}^* obey the orthonormal condition,

$$\int_0^{\pi}\int_0^{2\pi}Y_{lr}(\theta,\omega)Y_{lr}^*(\theta,\omega)\sin\theta\mathrm{d}\theta\mathrm{d}\omega=\delta_{ll'}\delta_{rr'}. \tag{A.2}$$

Define $\mu=\cos\theta$. The discrete ordinate directions in 3D case has the following forms,

$$\Omega_1=\mu,\quad \Omega_2=\sqrt{1-\mu^2}\cos\omega,\quad \Omega_3=\sqrt{1-\mu^2}\sin\omega. \tag{A.3}$$

$P_l^m(\mu)$ is the associated Legendre polynomials,

$$P_l^r(\mu)=\frac{(-1)^r}{2^l l!}(1-\mu^2)^{r/2}\frac{\mathrm{d}^{l+r}}{\mathrm{d}\mu^{l+r}}(\mu^2-1)^l,\quad P_l^{-r}(\mu)=(-1)^r\frac{(l-r)!}{(l+r)!}P_l^r(\mu),\quad |r|\le l.$$

$P_l^r(\mu)$ satisfies the following orthogonal relationship,

$$\frac{1}{2}\int_{-1}^{1}P_l^r(\mu)P_{l'}^{r'}(\mu)\mathrm{d}\mu=\frac{1}{2l+1}\frac{(l+r)!}{(l-r)!}\delta_{ll'}\delta_{rr'}. \tag{A.4}$$

And $P_l^r(\mu)$ has the following recurrence relations,

$$(2l+1)\mu P_l^r(\mu)=(l+r)P_{l-1}^r(\mu)+(l-r+1)P_{l+1}^r. \tag{A.5}$$

With Eq. (A.1), the collision term can be rewritten as,

$$S(\mathbf{x},t,\mathbf{\Omega},E)=\int\frac{\Sigma(\mathbf{x},E')}{\Sigma(\mathbf{x},E)}\sum_{l=0}^{L}\sum_{r=-l}^{l}f_l(\mathbf{x},E'\to E)Y_{lm}(\theta,\omega)\left(\int Y_{lm}^*(\theta',\omega')\phi(\mathbf{x},t,\mathbf{\Omega}',E')\mathrm{d}\mathbf{\Omega}'\right)\mathrm{d}E'.$$

Define

$$\varphi_{g,l}^{r}=\int Y_{lr}^{*}(\theta,\omega)\phi(\mathbf{x},t,\mathbf{\Omega},E)\mathrm{d}\mathbf{\Omega}. \tag{A.6}$$

The spherical harmonic expansion of the anisotropic collision term is,

$$S(\mathbf{x},t,\mathbf{\Omega},E)=\sum_{g'}\frac{\Sigma(\mathbf{x},E')}{\Sigma(\mathbf{x},E)}\sum_{l=0}^{L}\sum_{r=-l}^{l}f_l(\mathbf{x},E'\to E)Y_{lr}(\theta,\omega)\varphi_{g',l}^{r}.$$

Next, in order to have a more intuitive understanding of the collision term, we give the specific forms of Eq. (A) for low order models.

The expressions of the first few $P_l^m(\mu)$ are as,

$$\begin{aligned}
&P_0^0(\mu)=1,\\
&P_1^0(\mu)=\mu,\quad P_1^1(\mu)=-\sqrt{1-\mu^2},\\
&P_2^0(\mu)=\frac{3}{2}\mu^2-\frac{1}{2},\quad P_2^1(\mu)=-3\mu\sqrt{1-\mu^2},\quad P_2^2(\mu)=3(1-\mu^2).
\end{aligned}$$

Correspondingly, the low order $Y_{lm}(\theta,\omega)$ terms are,

$$\begin{aligned}
&Y_{00}(\theta,\omega)=\sqrt{\frac{1}{4\pi}},\\
&Y_{10}(\theta,\omega)=\sqrt{\frac{3}{4\pi}}\mu,\\
&Y_{11}(\theta,\omega)=-\sqrt{\frac{3}{8\pi}(1-\mu^2)}(\cos\omega+\mathrm{i}\sin\omega),\quad Y_{1-1}(\theta,\omega)=\sqrt{\frac{3}{8\pi}(1-\mu^2)}(\cos\omega-\mathrm{i}\sin\omega).
\end{aligned}$$

For isotropic case when $L=0$, it has,

$$S(\mathbf{x},t,\mathbf{\Omega},E)=\frac{1}{4\pi}\sum_{g'}\frac{\Sigma(\mathbf{x},E')}{\Sigma(\mathbf{x},E)}f_0(\mathbf{x},E'\to E)\varphi_{g'},$$

where define $\varphi_{g'}=\int\phi(\mathbf{x},t,\mathbf{\Omega},E)\mathrm{d}\mathbf{\Omega}$.

For $P1$ case when $L=1$, it has,

$$S(\mathbf{x},t,\mathbf{\Omega},E)=\sum_{g'}\frac{\Sigma(\mathbf{x},E')}{\Sigma(\mathbf{x},E)}\left(\frac{1}{4\pi}f_0(\mathbf{x},E'\to E)\varphi_{g'}+\frac{3}{4\pi}f_1(\mathbf{x},E'\to E)\sum_{i=1}^{3}\Omega_i\varphi_{g',i}^{(1)}\right),$$

where the moments of ϕ are defined as,

$$\varphi_{g',i}^{(1)}=\int\Omega_i\phi(\mathbf{x},t,\mathbf{\Omega},E)\mathrm{d}\mathbf{\Omega}.$$

For the $P2$ case with $L=2$, the related moments of $f_2(\mathbf{x},E'\to E)$ include,

$$<\Omega_1^2\phi>,\ <\Omega_2^2\phi>,\ <\Omega_3^2\phi>,\ <\Omega_1\Omega_2\phi>,\ <\Omega_1\Omega_3\phi>,\ <\Omega_2\Omega_3\phi>.$$

Here define the integral symbol $<\cdot>=\int\cdot\,\mathrm{d}\Omega$.

For the $P3$ case with $L=3$, the related moments of $f_3(\mathbf{x},E'\to E)$ include,

$$<\Omega_1^3\phi>,\ <\Omega_2^3\phi>,\ <\Omega_3^3\phi>,\ <\Omega_1^2\Omega_2\phi>,\ <\Omega_1^2\Omega_3\phi>,\ <\Omega_2^2\Omega_3\phi>,$$
$$<\Omega_1\Omega_2^2\phi>,\ <\Omega_1\Omega_3^2\phi>,\ <\Omega^2\Omega_3^2\phi>,\ <\Omega_1\Omega_2\Omega_3\phi>.$$

B Stability analysis of the L-th moment equation

In order to simplify the analysis process, we take the simplified model equation of one-dimensional single-group as an example to analyze the stability. For the P0 scattering model equation, suppose the distribution function of ϕ is,

$$\phi(\Omega)=\frac{A}{4\pi}\mathrm{e}^{ikx}.$$

It can be get,

$$\varphi^{(0)}=A\mathrm{e}^{ikx},\quad S(\Omega)=\frac{A\sigma_0}{4\pi}\mathrm{e}^{ikx}.$$

The transport equation of $\varphi^{(0)}$ is,

$$\frac{\partial\varphi^{(0)}}{\partial t}+\nabla\cdot\left(\int\Omega A\mathrm{e}^{ikx}\mathrm{d}\Omega\right)=\frac{\sigma_0-1}{\tau}A\mathrm{e}^{ikx}. \tag{B.1}$$

The space-time discrete form of Eq. (B.1) is,

$$\frac{\varphi^{(0),p+1}-\varphi^{(0),p}}{\Delta t}+\frac{F^{\phi}_{i+1/2}-F^{\phi}_{i-1/2}}{\Delta x}=\frac{\sigma_0-1}{\tau}\varphi^{(0),p+1}. \tag{B.2}$$

Here the collision term is implicitly discrete. Let $x_i=0$, and the flux at interface $i\pm1/2$ in the diffusion limit is,

$$\mathcal{F}^{(0)}_{i-1/2}=-\frac{1}{3}\tau v^2\sigma_0\frac{A(1-\mathrm{e}^{-ik\Delta x})}{\Delta x},$$
$$\mathcal{F}^{(0)}_{i+1/2}=-\frac{1}{3}\tau v^2\sigma_0\frac{A(\mathrm{e}^{ik\Delta x}-1)}{\Delta x}.$$

By substituting the numerical flux into Eq. (B.2), it can be get,

$$\varphi^{(0),p+1}=\left(\frac{1}{\Delta t}+\frac{1-\sigma_0}{\tau}\right)^{-1}\left[\frac{1}{3}\tau v^2\sigma_0\frac{A\mathrm{e}^{ik\Delta x}+A\mathrm{e}^{-ik\Delta x}-2A}{\Delta x^2}+\frac{A}{\Delta t}\right].$$

The magnification factor G is,

$$|G|=\left(\frac{1}{\Delta t}+\frac{1-\sigma_0}{\tau}\right)^{-1}\left|\frac{2}{3}\tau v^2\sigma_0\frac{\cos(k\Delta x)-1}{\Delta x^2}+\frac{1}{\Delta t}\right|\le\left|1-\frac{4}{3}\frac{\tau v^2\sigma_0}{\Delta x^2}\sin^2\left(\frac{k\Delta x}{2}\right)\right|.$$

Thus, the constraint condition of Δt is,

$$\Delta t \leq \frac{3\Sigma\Delta x^2}{2\sigma_0 v}.$$

For the P1 scattering model equation, ϕ is assumed to be,

$$\phi_m = \frac{A}{4\pi} e^{ikx} \Omega_m.$$

Then the expressions of $\varphi^{(*)}$ and $S(\Omega)$ are,

$$\varphi^{(0)} = 0, \quad \varphi^{(1)} = \frac{A}{3} e^{ikx}, \quad S = \frac{A}{4\pi} \sigma_1 e^{ikx} \Omega_m.$$

And the equation of $\varphi^{(1)}$ is,

$$\frac{\partial \varphi^{(1)}}{\partial t} + \nabla \cdot \left(\int \Omega^2 \phi \mathrm{d}\Omega \right) = \frac{\sigma_1 - 1}{\tau} \varphi^{(1)}.$$

Similar to the derivation of P0 model equation, the numerical flux of interface $i \pm 1/2$ in the diffusion limit is,

$$\mathcal{F}^{(1)}_{i-1/2} = -\frac{1}{5}\tau v^2 \sigma_1 \frac{A(1 - e^{-ik\Delta x})}{\Delta x},$$
$$\mathcal{F}^{(1)}_{i+1/2} = -\frac{1}{5}\tau v^2 \sigma_1 \frac{A(e^{ik\Delta x} - 1)}{\Delta x}.$$

We can easily get that the stability condition of P1 scattering model equation is,

$$\Delta t \leq \min\left(\frac{3\Sigma\Delta x^2}{2\sigma_0 v}, \frac{5\Sigma\Delta x^2}{6\sigma_1 v} \right).$$

Therefore, through simple analysis, the constraint condition for the L-order scattering term is,

$$\Delta t \leq \begin{cases} \frac{(L+3)\Sigma\Delta x^2}{2(L+1)\sigma_L v}, & L = 0,2,4,\cdots, \\ \frac{(L+4)\Sigma\Delta x^2}{2(L+2)\sigma_L v}, & L = 1,3,5,\cdots. \end{cases} \tag{B.3}$$

The limit value of Eq. (B.3) is,

$$\Delta t \leq \frac{\Sigma\Delta x^2}{2v \max(\sigma_0, \sigma_1, \cdots, \sigma_L)}. \tag{B.4}$$

C Moments of collision term

Define the integral operation symbol $<\cdot>=\int\cdot\,\mathrm{d}\Omega$. For anisotropic scattering model equation, the 1st moments of S are,

$$<\Omega_i S>=\sum_{g'}\sum_{l=0}^{L}\sigma_l(\mathbf{x},E'\to E)\sum_{m=-l}^{l}\varphi_{g',l}^{m}\int\Omega_i Y_{lm}(\theta,\omega)\mathrm{d}\Omega.$$

For the l-th order, the angular integral term is,

$$\begin{aligned}
&\sum_{m=-l}^{l}\varphi_{g',l}^{m}\int\Omega_i Y_{lm}(\theta,\omega)\mathrm{d}\Omega\\
=&\frac{2l+1}{4\pi}\varphi_{g',l}^{0}\int\Omega_i P_l^0(\mu)\mathrm{d}\Omega\\
&+\sum_{m=1}^{l}\left[\frac{(2l+1)(l-m)!}{4\pi(l+m)!}\right]\left(\varphi_{g,l}^{m,R}-i\varphi_{g,l}^{m,I}\right)\int\Omega_i P_l^m(\mu)\mathrm{e}^{im\omega}\mathrm{d}\Omega\\
&+\sum_{m=1}^{l}\left[\frac{(2l+1)(l-m)!}{4\pi(l+m)!}\right]\left(\varphi_{g,l}^{m,R}+i\varphi_{g,l}^{m,I}\right)\int\Omega_i P_l^m(\mu)\mathrm{e}^{-im\omega}\mathrm{d}\Omega.
\end{aligned}\tag{C.1}$$

Here the moments of $\varphi_{g,l}^{m,R}$ and $\varphi_{g,l}^{m,I}$ are defined as,

$$\begin{aligned}
\varphi_{g,l}^{m,R}&=\int P_l^m(\mu)\cos(m\omega)\phi(\mathbf{x},t,\mathbf{\Omega},E)\mathrm{d}\Omega,\\
\varphi_{g,l}^{m,I}&=\int P_l^m(\mu)\sin(m\omega)\phi(\mathbf{x},t,\mathbf{\Omega},E)\mathrm{d}\Omega.
\end{aligned}$$

The components of $\int\Omega_i P_l^m(\mu)\mathrm{e}^{\pm im\omega}\mathrm{d}\Omega$ are,

$$\begin{aligned}
&\int\Omega_1 P_l^m(\mu)\mathrm{e}^{\pm im\omega}\mathrm{d}\Omega=\int\mu P_l^m(\mu)\mathrm{d}\mu\int(\cos(m\omega)\pm i\sin(m\omega))\mathrm{d}\omega=0,\\
&\int\Omega_2 P_l^m(\mu)\mathrm{e}^{\pm im\omega}\mathrm{d}\Omega=\begin{cases}\pi\int\sqrt{1-\mu^2}P_l^1(\mu)\mathrm{d}\mu, & m=1;\\ 0, & \text{else},\end{cases}\\
&\int\Omega_3 P_l^m(\mu)\mathrm{e}^{\pm im\omega}\mathrm{d}\Omega=\begin{cases}\pm i\pi\int\sqrt{1-\mu^2}P_l^1(\mu)\mathrm{d}\mu, & m=1;\\ 0, & \text{else}.\end{cases}
\end{aligned}$$

Thus, Eq. (C.1) can be simplified as,

$$\begin{aligned}
&\sum_{m=-l}^{l}\varphi_{g',l}^{m}\int\Omega_1 Y_{lm}(\theta,\omega)\mathrm{d}\Omega=\frac{2l+1}{2}\varphi_{g',l}^{0}\int\Omega_1 P_l^0(\mu)\mathrm{d}\mu,\\
&\sum_{m=-l}^{l}\varphi_{g',l}^{m}\int\Omega_2 Y_{lm}(\theta,\omega)\mathrm{d}\Omega=\frac{2l+1}{2l(l+1)}\varphi_{g,l}^{1,R}\int\sqrt{1-\mu^2}P_l^1(\mu)\mathrm{d}\mu,\\
&\sum_{m=-l}^{l}\varphi_{g',l}^{m}\int\Omega_3 Y_{lm}(\theta,\omega)\mathrm{d}\Omega=\frac{2l+1}{2l(l+1)}\varphi_{g,l}^{1,I}\int\sqrt{1-\mu^2}P_l^1(\mu)\mathrm{d}\mu.
\end{aligned}$$

According to the orthogonal relation in Eq. (A.4), it can be further simplified as,

$$\begin{aligned}
<\Omega_1 S> &= \sum_{g'} \sigma_{1,g'\to g} <\Omega_1 \phi_{g'}>, \\
<\Omega_2 S> &= \sum_{g'} \sigma_{1,g'\to g} <\Omega_2 \phi_{g'}>, \\
<\Omega_3 S> &= \sum_{g'} \sigma_{1,g'\to g} <\Omega_3 \phi_{g'}>.
\end{aligned}$$

The 2nd moments of S are,

$$<\Omega_i\Omega_j S> = \sum_{g'}\sum_{l=0}^{L} \sigma_l(\mathbf{x}, E'\to E) \sum_{m=-l}^{l} \varphi^m_{g',l} \int \Omega_i\Omega_j Y_{lm}(\theta,\omega)\mathrm{d}\Omega.$$

For the 2nd order, the angular integral term is,

$$\begin{aligned}
&\sum_{m=-l}^{l} \varphi^m_{g',l} \int \Omega_i\Omega_j Y_{lm}(\theta,\omega)\mathrm{d}\Omega \\
=&\frac{2l+1}{4\pi}\varphi^0_{g',l}\int \Omega_i\Omega_j P^0_l(\mu)\mathrm{d}\Omega \\
&+\sum_{m=1}^{l}\left[\frac{(2l+1)(l-m)!}{4\pi(l+m)!}\right]\left(\varphi^{m,R}_{g,l} - i\varphi^{m,I}_{g,l}\right)\int \Omega_i\Omega_j P^m_l(\mu)\mathrm{e}^{im\omega}\mathrm{d}\Omega \\
&+\sum_{m=1}^{l}\left[\frac{(2l+1)(l-m)!}{4\pi(l+m)!}\right]\left(\varphi^{m,R}_{g,l} + i\varphi^{m,I}_{g,l}\right)\int \Omega_i\Omega_j P^m_l(\mu)\mathrm{e}^{-im\omega}\mathrm{d}\Omega. \qquad \text{(C.2)}
\end{aligned}$$

The components of $\int \Omega_i\Omega_j P^m_l(\mu)\mathrm{e}^{\pm im\omega}\mathrm{d}\Omega$ are,

$$\begin{aligned}
\int \Omega_1^2 P^m_l(\mu)\mathrm{e}^{\pm im\omega}\mathrm{d}\Omega &= \int \mu^2 P^m_l(\mu)\mathrm{d}\mu \int (\cos(m\omega)\pm i\sin(m\omega))\mathrm{d}\omega = 0, \\
\int \Omega_1\Omega_2 P^m_l(\mu)\mathrm{e}^{\pm im\omega}\mathrm{d}\Omega &= \begin{cases} \pi\int \mu\sqrt{1-\mu^2}P^1_l(\mu)\mathrm{d}\mu, & m=1; \\ 0, & \text{else}, \end{cases} \\
\int \Omega_1\Omega_3 P^m_l(\mu)\mathrm{e}^{\pm im\omega}\mathrm{d}\Omega &= \begin{cases} \pm i\pi\int \mu\sqrt{1-\mu^2}P^1_l(\mu)\mathrm{d}\mu, & m=1; \\ 0, & \text{else}, \end{cases} \\
\int \Omega_2^2 P^m_l(\mu)\mathrm{e}^{\pm im\omega}\mathrm{d}\Omega &= \begin{cases} \frac{\pi}{2}\int (1-\mu^2)P^2_l(\mu)\mathrm{d}\mu, & m=2; \\ 0, & \text{else}, \end{cases} \\
\int \Omega_2\Omega_3 P^m_l(\mu)\mathrm{e}^{\pm im\omega}\mathrm{d}\Omega &= \begin{cases} \pm i\frac{\pi}{2}\int (1-\mu^2)P^2_l(\mu)\mathrm{d}\mu, & m=2; \\ 0, & \text{else}, \end{cases} \\
\int \Omega_3^2 P^m_l(\mu)\mathrm{e}^{\pm im\omega}\mathrm{d}\Omega &= \begin{cases} -\frac{\pi}{2}\int (1-\mu^2)P^2_l(\mu)\mathrm{d}\mu, & m=2; \\ 0, & \text{else}. \end{cases}
\end{aligned}$$

Eq. (C.2) is rearranged as,

$$\begin{aligned}
\sum_{m=-l}^{l}\varphi_{g',l}^{m}\int\Omega_1^2Y_{lm}(\theta,\omega)\mathrm{d}\Omega&=\frac{2l+1}{2}\varphi_{g',l}^{0}\int\Omega_1^2P_l^0(\mu)\mathrm{d}\mu,\\
\sum_{m=-l}^{l}\varphi_{g',l}^{m}\int\Omega_1\Omega_2Y_{lm}(\theta,\omega)\mathrm{d}\Omega&=\frac{2l+1}{2l(l+1)}\varphi_{g,l}^{1,R}\int\mu\sqrt{1-\mu^2}P_l^1(\mu)\mathrm{d}\mu,\\
\sum_{m=-l}^{l}\varphi_{g',l}^{m}\int\Omega_1\Omega_3Y_{lm}(\theta,\omega)\mathrm{d}\Omega&=\frac{2l+1}{2l(l+1)}\varphi_{g,l}^{1,I}\int\mu\sqrt{1-\mu^2}P_l^1(\mu)\mathrm{d}\mu,\\
\sum_{m=-l}^{l}\varphi_{g',l}^{m}\int\Omega_2^2Y_{lm}(\theta,\omega)\mathrm{d}\Omega&=\frac{2l+1}{4}\varphi_{g',l}^{0}\int(1-\mu^2)P_l^0(\mu)\mathrm{d}\mu\\
&\quad+\frac{(2l+1)(l-2)!}{4(l+2)!}\varphi_{g,l}^{2,R}\int(1-\mu^2)P_l^2(\mu)\mathrm{d}\mu,\\
\sum_{m=-l}^{l}\varphi_{g',l}^{m}\int\Omega_2\Omega_3Y_{lm}(\theta,\omega)\mathrm{d}\Omega&=\frac{(2l+1)(l-2)!}{4(l+2)!}\varphi_{g,l}^{2,I}\int(1-\mu^2)P_l^2(\mu)\mathrm{d}\mu,\\
\sum_{m=-l}^{l}\varphi_{g',l}^{m}\int\Omega_3^2Y_{lm}(\theta,\omega)\mathrm{d}\Omega&=\frac{2l+1}{4}\varphi_{g',l}^{0}\int(1-\mu^2)P_l^0(\mu)\mathrm{d}\mu\\
&\quad+\frac{(2l+1)(l-2)!}{4(l+2)!}\varphi_{g,l}^{2,R}\int(1-\mu^2)P_l^2(\mu)\mathrm{d}\mu.
\end{aligned}$$

Combined with the orthogonal relation in Eq. (A.4), the integral term of μ has the following forms,

$$\begin{aligned}
&\int\mu^2P_0^0(\mu)\mathrm{d}\mu=\frac{2}{3},\\
&\int\mu^2P_2^0(\mu)\mathrm{d}\mu=\frac{4}{15},\\
&\int\mu\sqrt{1-\mu^2}P_2^1(\mu)\mathrm{d}\mu=-\frac{4}{5},\\
&\int(1-\mu^2)P_0^0(\mu)\mathrm{d}\mu=\frac{4}{3},\\
&\int(1-\mu^2)P_2^0(\mu)\mathrm{d}\mu=-\frac{4}{15},\\
&\int(1-\mu^2)P_2^2(\mu)\mathrm{d}\mu=\frac{16}{5}.
\end{aligned}$$

Thus, $<\Omega_i\Omega_j S>$ can be simplified as,

$$\sum_{m=-l}^{l}\varphi_{g',l}^{m}\int\Omega_1^2Y_{lm}(\theta,\omega)\mathrm{d}\Omega=\frac{1}{3}\sum_{g'}(\sigma_{0,g'\to g}-\sigma_{2,g'\to g})\varphi_{g'}+\sum_{g'}\sigma_{2,g'\to g}<\Omega_1\Omega_1\phi_{g'}>,$$

$$\sum_{m=-l}^{l}\varphi_{g',l}^{m}\int\Omega_1\Omega_2Y_{lm}(\theta,\omega)\mathrm{d}\Omega=\sum_{g'}\sigma_{2,g'\to g}<\Omega_1\Omega_2\phi_{g'}>,$$

$$\sum_{m=-l}^{l}\varphi_{g',l}^{m}\int\Omega_1\Omega_3Y_{lm}(\theta,\omega)\mathrm{d}\Omega=\sum_{g'}\sigma_{2,g'\to g}<\Omega_1\Omega_3\phi_{g'}>,$$

$$\sum_{m=-l}^{l}\varphi_{g',l}^{m}\int\Omega_2^2Y_{lm}(\theta,\omega)\mathrm{d}\Omega=\frac{1}{3}\sum_{g'}(\sigma_{0,g'\to g}-\sigma_{2,g'\to g})\varphi_{g'}+\sum_{g'}\sigma_{2,g'\to g}<\Omega_2\Omega_2\phi_{g'}>,$$

$$\sum_{m=-l}^{l}\varphi_{g',l}^{m}\int\Omega_2\Omega_3Y_{lm}(\theta,\omega)\mathrm{d}\Omega=\sum_{g'}\sigma_{2,g'\to g}<\Omega_2\Omega_3\phi_{g'}>,$$

$$\sum_{m=-l}^{l}\varphi_{g',l}^{m}\int\Omega_3^2Y_{lm}(\theta,\omega)\mathrm{d}\Omega=\frac{1}{3}\sum_{g'}(\sigma_{0,g'\to g}-\sigma_{2,g'\to g})\varphi_{g'}+\sum_{g'}\sigma_{2,g'\to g}<\Omega_3\Omega_3\phi_{g'}>.$$

D Model parameters for KAPL

For region void, Σ_g, $g=1,2,3$ is set as 10^{-20} avoid singularity in numerical calculation. And other cross section parameters are all zero.

Table 8: The three group total cross section parameters for KAPL.

Region	Group 1	Group 2	Group 3
Source region(I)	1.5209e-1	2.4414e-1	4.7510e-1
Side iron(II)	3.0853e-1	2.6767e-1	2.4658e-1
Iron outside(III)	3.0792e-1	2.6399e-1	2.4460e-1
Side water(IV)	1.4939e-1	2.5480e-1	4.9522e-1
Bottom water(V)	1.5080e-1	2.4224e-1	4.7529e-1
Central water(VI)	1.5061e-1	2.4215e-1	4.7527e-1
Upper iron(VII)	3.0311e-1	2.6876e-1	2.4545e-1
Outer water(VIII)	1.3791e-1	2.5307e-1	4.9833e-1

Table 9: Three group P0 cross sections for KAPL.

Region	$\Sigma_{s,0}$	Group 1	Group 2	Group 3
Source region(I)	$g\to1$	5.50690e-2	–	–
	$g\to2$	6.62270e-2	1.14080e-1	–
	$g\to3$	2.81535e-2	1.30005e-1	4.75098e-1
Side iron(II)	$g\to1$	1.81200e-1	–	–
	$g\to2$	6.74630e-2	2.11630e-1	–
	$g\to3$	5.65677e-2	5.56596e-2	2.46217e-1
Iron outside(III)	$g\to1$	1.81040e-1	–	–
	$g\to2$	6.73630e-2	2.04540e-1	–
	$g\to3$	5.61202e-2	5.91218e-2	2.44224e-1
Side water(IV)	$g\to1$	5.62070e-2	–	–
	$g\to2$	6.33120e-2	1.02380e-1	–
	$g\to3$	2.71698e-2	1.52391e-1	4.95218e-1
Bottom water(V)	$g\to1$	5.57300e-2	–	–
	$g\to2$	6.47110e-2	1.14970e-1	–
	$g\to3$	2.77104e-2	1.27214e-1	4.75288e-1
Central water(VI)	$g\to1$	5.58200e-2	–	–
	$g\to2$	6.44960e-2	1.15030e-1	–
	$g\to3$	2.76445e-2	1.27071e-1	4.75270e-1
Upper iron(VII)	$g\to1$	1.82500e-1	–	–
	$g\to2$	6.52940e-2	2.13570e-1	–
	$g\to3$	5.10076e-2	5.47906e-2	2.45084e-1
Outer water(VIII)	$g\to1$	6.11190e-2	–	–
	$g\to2$	5.08650e-2	1.04630e-1	–
	$g\to3$	2.29312e-2	1.48405e-1	4.98329e-1

Table 10: Three group P1 cross sections for KAPL.

Region	$\Sigma_{s,1}$	Group 1	Group 2	Group 3
Source region(I)	$g\to1$	3.4757e-2	–	–
	$g\to2$	3.7043e-2	6.7420e-2	–
	$g\to3$	9.37598e-3	6.29807e-2	2.41101e-1
Side iron(II)	$g\to1$	1.3024e-1	–	–
	$g\to2$	-2.0035e-4	6.9070e-2	–
	$g\to3$	0.0e0	-2.1840e-3	5.5863e-2
Iron outside(III)	$g\to1$	1.3022e-1	–	–
	$g\to2$	-1.9907e-4	6.5533e-2	–
	$g\to3$	0.0e0	-2.8134e-3	5.61362e-2
Side water(IV)	$g\to1$	3.4923e-2	–	–
	$g\to2$	3.6120e-2	6.0000e-2	–
	$g\to3$	9.12651e-3	7.60892e-2	2.56796e-1
Bottom water(V)	$g\to1$	3.4757e-2	–	–
	$g\to2$	3.7043e-2	6.7420e-2	–
	$g\to3$	9.37598e-3	6.29807e-2	2.41101e-1
Central water(VI)	$g\to1$	3.4780e-2	–	–
	$g\to2$	3.6930e-2	6.7457e-2	–
	$g\to3$	9.34568e-3	6.29077e-2	2.41093e-1
Upper iron(VII)	$g\to1$	1.3089e-1	–	–
	$g\to2$	-1.0523e-4	7.0373e-2	–
	$g\to3$	0.0d0	-2.0437e-3	5.58192e-2
Outer water(VIII)	$g\to1$	3.6483e-2	–	–
	$g\to2$	2.8960e-2	6.1280e-2	–
	$g\to3$	7.22521e-3	7.39963e-2	2.58898e-1

References

[1] S. Tan, W. Sun, J. Wei, G. Ni, A parallel unified gas kinetic scheme for three-dimensional multi-group neutron transport, J. Comput. Phys., 391 (2019), 37–58.

[2] S. Tan, W. Sun, K. Xu, J. Wei, G. Ni, Time implicit unified gas kinetic scheme for 3D multi-group neutron transport simulation, Commun. Comput. Phys., 28 (3) (2020), 1189–1218.

[3] C. Liu, X.-L. Hu, B. Zhang, Y. Gong, L. Zhang, Y.-X. Chen, Numerical study of scattering Legendre moments and effect of anisotropic scattering on S_n shielding calculation, Nucl. Sci. Tech., 30 (11) (2019), 161.

[4] L. Chacon, G. Chena, D. A. Knoll, C. Newman, H. Park, W. Taitano, J. A. Willert, G. Womeldorff, Multiscale high-order/low-order (HOLO) algorithms and applications, J. Comput. Phys., 330 (2017), 21–45.

[5] E. Larsen, A grey transport acceleration method for time-dependent radiative transfer problems, J. Comput. Phys., 78 (2) (1988), 459–480.

[6] G. L. Ramone, M. L. Adams, P. F. Nowak, A transport synthetic acceleration method for transport iterations, Nucl. Sci. Eng., 125 (3) (1997), 257–283.

[7] E. Larsen, Transport acceleration methods as two-level multigrid algorithms, Modern Mathematical Methods in Transport Theory, 1991, pp. 34–47.

[8] E. Larsen, J. Morel, J. Miller, Asymptotic solutions of numerical transport problems in optically thick, diffusive regimes, J. Comput. Phys., 69 (2) (1987), 283–324.

[9] S. Jin, D. Levermore, The discrete-ordinate method in diffusive regimes, Transport. Theor. Stat., 20 (5-6) (1991), 413–439.

[10] S. Jin, D. Levermore, Fully-discrete numerical transfer in diffusive regimes, Transport. Theor. Stat., 22 (6) (1993) 739–791.

[11] J. Hu, S. Jin, Q. Li, Asymptotic-preserving schemes for multiscale hyperbolic and kinetic equations, in: Handbook of Numerical Analysis, Vol. 18, Elsevier, 2017, pp. 103–129.

[12] R. Sanchez, J. Ragusa, E. Masiello, Asymptotic theory of the linear transport equation in anisotropic media, J. Math. Phys., 49 (8) (2008), 083504–1–18.

[13] L. Wang, B. Yan, An asymptotic-preserving scheme for the kinetic equation with anisotropic scattering: Heavy tail equilibrium and degenerate collision frequency, SIAM. J. Sci. Comput., 41 (1) (2019), A422–A451.

[14] K. Xu, J.-C. Huang, A unified gas-kinetic scheme for continuum and rarefied flows, J. Comput. Phys., 229 (20) (2010), 7747–7764.

[15] J.-C. Huang, K. Xu, P. Yu, A unified gas-kinetic scheme for continuum and rarefied flows II: Multi-dimensional cases, Commun. Comput. Phys., 12 (3) (2012), 662–690.

[16] S. Chen, K. Xu, A comparative study of an asymptotic preserving scheme and unified gas-kinetic scheme in continuum flow limit, J. Comput. Phys., 288 (2015), 52–65.

[17] L. Mieussens, On the asymptotic preserving property of the unified gas kinetic scheme for the diffusion limit of linear kinetic models, J. Comput. Phys., 253 (2013), 138–156.

[18] W. Sun, S. Jiang, K. Xu, An asymptotic preserving unified gas kinetic scheme for gray radiative transfer equations, J. Comput. Phys., 285 (2015), 265–279.

[19] W. Sun, S. Jiang, K. Xu, S. Li, An asymptotic preserving unified gas kinetic scheme for frequency-dependent radiative transfer equations, J. Comput. Phys., 302 (2015), 222–238.

[20] L. Zhu, Z. Guo, K. Xu, Discrete unified gas kinetic scheme on unstructured meshes, Comput. Fluids., 127 (2016), 211–225.

[21] X. Zhou, Z. Guo, Discrete unified gas kinetic scheme for steady multiscale neutron transport, J. Comput. Phys., 423 (2020), 109767.

[22] X. Song, C. Zhang, X. Zhou, Z. Guo, Discrete unified gas kinetic scheme for multiscale anisotropic radiative heat transfer, Adv. Aerodyn., 2 (3) (2020), 1–15.
[23] S. Yoon, A. Jameson, Lower-upper symmetric-gauss-seidel method for the Euler and Navier-Stokes equations, AIAA J., 26 (9) (1988), 1025–1026.
[24] Q. Li, L. Wang, Implicit asymptotic preserving method for linear transport equations, Commun. Comput. Phys. 22 (1) (2017), 157–181.
[25] T.-K. Kim, H. Lee, Effect of anisotropic scattering on radiative heat transfer in two-dimensional rectangular enclosures, Int. J. Heat. Mass. Tran., 31 (8) (1988), 1711–1721.
[26] N. S. Riyait, R. T. Ackroyd, The finite-element method for multigroup neutron transport: Anisotropic scattering in 1-D slab geometry, Ann. Nucl. Energy., 14 (3) (1987), 113–133.
[27] C. S. Quah, A comparison of finite elements and discrete ordinate methods for one-dimensional multigroup problems, Ann. Nucl. Energy., 8 (11-12), (1981) 709–715.
[28] T. Asaoka, N. Asano, H. Nakamura, H. Mizuta, H. Chichiwa, T. Ohnishi, S. I. Miyasaka, A. Zukeran, T. Tsutsui, T. Fujimura, S. Katsuragi, Benchmark tests of radiation transport computer codes for reactor core and shield calculations, J. Nucl. Sci. Technol., 15 (1) (1978), 56–71.
[29] N. S. Riyait, Anisotropic scattering, voids and hybrid principles in finite element neutron transport., Ph.D. thesis, 1988.